MM

RESEARCH ON THE SAILRAIL COMPLIANT SURFACE AIR BEARING

Project Team:

M. J. Hinchey, P. A. Sullivan and T. A. Graham

TP 2817

Transport Canada / Transports Canada
Library and Information Centre /
Centre de Documentation GSLA
Ottawa, Canada K1A 0N5

for

Transportation Development Centre
Transport Canada
Montreal, Quebec

TDC File D-500-599-1

January, 1981

The contents of this report reflect the views of the contractor and not necessarily the official views or policies of the Transportation Development Centre.

Transport Canada | Transports Canada
Library and Information Centre
Centre de Documentation
Ottawa, Canada K1A 0N5

REPORT DOCUMENTATION FORM

1. Transport Canada Report No.	2. TDC Project No.	3. Recipient's Catalogue No.
TP2817	4054	

4. Title and Subtitle	5. Report Date
RESEARCH ON THE SAILRAIL COMPLIANT SURFACE AIR BEARING	January 1981
	6. Performing Organization Report No.

7. Author(s)	8. Transport Canada File No.
M.J. Hinchey, P.A. Sullivan, T.A. Graham	D-500-599-1

9. Performing Organization Name and Address	10. DSS File No.
University of Toronto Institute for Aerospace Studies 4925 Dufferin Street Downsview, Ontario M3H 5T6	T8200-9-9522
	11. DSS or Transport Canada Contract No.
	1SD79-00084

12. Sponsoring Agency Name and Address	13. Type of Report and Period Covered
Transportation Development Centre (TDC) 1000 Sherbrooke Street West P.O. Box 549, Place de l'aviation Montreal, Quebec H3A 2R3	Final
	14. Sponsoring Agency Code
	4054

15. Supplementary Notes	16. TDC Project Officer
	J.E. Laframboise

17. Abstract

A one year study of the behaviour of a palletized goods handling system that uses a cellulosic shoe sliding on concave rails is described. Air under pressure is injected between the shoe and the rail through holes drilled in the rail surface. Measurements were made of the depth of the cavity between rail surface and the shoe, and the flow of air around the injector holes was observed. A mathematical model of the shoe pressure distribution was established through finite element flow analysis.

Qualitative agreement was observed between predicted and observed pressure distribution, indicating that the complex shoe structure behaved as a conventional resilient air bearing. Subsequent studies proposed would strive to simplify the system and improve its load bearing capacity.

18. Key Words	19. Distribution Statement
Compliant air bearing, air cushion handling of pallets, intermodale goods handling	Limited number of copies available from Transportation Development Centre

20. Security Classification (of this report)	21. Security Classification (of this page)	22. No. of Pages	23. Price
Nil	Nil	45 + 5 app.	Nil

FORMULE DE DOCUMENTATION POUR RAPPORT

1. N° du rapport Transports Canada	2. N° de l'étude — CDT	3. N° de catalogue du destinataire
TP2817	4054	

4. Titre et sous-titre	5. Date du rapport
RESEARCH ON THE SAILRAIL COMPLIANT SURFACE AIR BEARING	janvier 1981
	6. N° du rapport de l'organisme exécutant

7. Auteur(s)	8. N° de dossier Transports Canada
M.J. Hinchey, P.A. Sullivan, T.A. Graham	D-500-599-1

9. Nom et adresse de l'organisme exécutant	10. N° de dossier — ASC
Institut d'études aérospatiales Université de Toronto 4925 rue Dufferin Downsview, Ontario M3H 5T6	T8200-9-9522
	11. N° de contrat — ASC ou Transports Canada
	1SD79-00084

12. Nom et adresse de l'organisme parrain	13. Genre de rapport et période visée
Centre de développement des transports (CDT) 1000, rue Sherbrooke ouest C.P. 549, Place de l'aviation Montréal (Québec) H3A 2R2	Final
	14. Code de l'organisme parrain
	4054

15. Remarques additionnelles	16. Agent de projet — CDT
	J.E. Laframboise

17. Résumé

Le rapport décrit le résultat d'une étude sur le comportement d'un système de manutention de marchandises sur palets, utilisant un sabot cellulosique glissant sur rails concaves. De l'air sous pression est injecté entre le rail et le sabot par des trous percés dans le fond du rail. On a mesuré la profondeur de la cavité entre le sabot et le rail et observé le déplacement de l'air autour des injecteurs. Un modèle mathématique de la distribution de la pression sous le sabot a été établi par l'analyse par éléments finis du courant fluide.

Un accord qualitatif existe entre les résultats de l'analyse et les mesures exécutées en laboratoire, indiquant que, malgré sa structure complexe, le sabot cellulosique se comporte comme un palier fluide élastique. Des études subséquentes sont proposées afin de simplifier le système et d'augmenter sa capacité de charge.

18. Mots-clés	19. Diffusion
Palier élastique aérostatique, manutention de palets sur coussin d'air, manutention intermodale	Nombre limité de copies disponibles auprès du Centre de développement des transports (CDT)

20. Classification de sécurité (de ce rapport)	21. Classification de sécurité (de cette page)	22. Nombre de pages	23. Prix
Aucune	Aucune	45 + 5 annexes	Nil

CDT/TDC 79-005

SailRail is a simple and rugged compliant air bearing device currently being developed by a Division of E. B. Eddy Forest Products, SailRail Enterprises, to facilitate and automate the movement and storage of goods carried on pallets in certain transport systems. The air bearing feature enables 1.3 m x 1.3 m pallets carrying loads up to 2000 kg to be moved by extremely small forces, typically one man can push a single loaded pallet. It appears especially suited to systems requiring the use of more than one mode and offers the possibility of effecting large economies in transportation system costs. For example, it has been successfully demonstrated that a single fork-lift truck can be used to tow the entire load of a typical highway trailer onto a warehouse dock in less than half a minute. The concept employs two shoes having an elliptic cross-section, which are about 0.16m wide by 1.3m long, and are attached to the underside edges of each pallet. The shoes, which are made of a highly compliant material, mate with 0.16m wide rails which appear as shallow grooves in the surface over which the loads are to be moved. Air for the bearing action is supplied by 0.75mm diameter holes in the rails spaced about 0.15m apart from manifolds integrated with rail section. The shoes also have a large vibration isolation capacity; this may be extremely important for some applications. The report describes the results of a one-year programme of research aimed at providing a basis for optimizing the design. Measurements of the gap distribution between shoe and rail are presented. These measured gap distributions are used in a numerical analysis of the air flow processes involved. The air flow is assumed to be planar and governed by the compressible Reynolds equation of hydrostatic lubrication, that is, pressure forces balance laminar viscous forces directly. The air supply holes are modelled as constant pressure sources. Comparison of computed pressure distributions with experimentally measured pressures shows good qualitative agreement. Work on the development of flow visualization techniques to help ascertain the effectiveness of air distribution under the shoes is also described. Areas of future work are identified.

TABLE OF CONTENTS

1. INTRODUCTION 1

1.1 BACKGROUND 1

1.2 THE SAILRAIL CONCEPT 1

1.3 RELATIONSHIP TO EXISTING GAS BEARING CONCEPTS 2

1.4 OBJECTIVES OF THE PRESENT WORK 3

2. THEORETICAL DEVELOPMENT 6

2.1 DISCUSSIONS OF THE POSSIBILITIES FOR ANALYSES 6

2.2 BRIEF DESCRIPTION OF THE FINITE ELEMENT ANALYSIS 7

3. DESCRIPTION OF EXPERIMENTAL FACILITIES 9

3.1 GAP MEASUREMENT FACILITY 9

3.2 FLOW PATTERN FACILITY 9

3.3 PROTOTYPE TEST BED 10

4. RESULTS 12

4.1 MEASURED GAP AND PRESSURE PROFILES 12

4.2 QUALITATIVE COMPARISONS WITH THEORETICAL PRESSURE PROFILES FOR SPECIFIC GAP DISTRIBUTION 13

4.3 FLOW PATTERNS 13

4.4 INITIAL RESULTS FROM PROTOTYPE TEST BED 14

4.5 DISCUSSION 15

5. CONCLUSIONS AND SUGGESTIONS FOR FUTURE WORK 16

5.1 CONCLUSIONS 16

5.2 SUGGESTIONS FOR FUTURE WORK 17

REFERENCES 20

FIGURES FOR MAIN TEXT

APPENDICES

APPENDIX A: DETAILS OF FINITE ELEMENT ANALYSIS

A.1 THE FINITE ELEMENT METHOD

A.2 GOVERNING EQUATION FOR AIR FLOW

A.3 APPLICATION OF GALERKIN'S METHOD

A.3.1 Elements

A.3.2 Integral Evaluations

A.3.3 Assembly of Contribution into Global Matrix

A.3.4 Boundary Conditions

A.3.5 Gauss Seidel Iteration

REFERENCES - APPENDIX A

APPENDIX B: LONGITUDINAL SLOT SOURCE: ANALYTICAL SOLUTION

APPENDIX C: STATIC PITCH STIFFNESS EXPERIMENT

APPENDIX D: CALIBRATION OF VARIOUS INSTRUMENTS

D.1 LINEAR VARIABLE DISPLACEMENT TRANSDUCER (LVDT)

D.2 LOAD CELLS

D.3 FLOW METERS (ROTAMETERS)

APPENDIX E: FINITE ELEMENT COMPUTER PROGRAMME

LIST OF FIGURES: MAIN TEXT

Fig. 1a	Trailer-warehouse system.	21
Fig. 1b	Trailer interior.	21
Fig. 2	Cross-section of track and shoe.	22
Fig. 3	Standard feed hole pattern.	22
Fig. 4	Possible gap feed hole configurations.	23
Fig. 5	Compliant surface air bearing.	23
Fig. 6	Prototype shoe pressure distribution.	24
Fig. 7	Hydrostatic lubrication geometry.	25
Fig. 8	Schematics of gap measurement facility.	26
Fig. 9	Pictures of gap measurement facility.	27
Fig. 10	Probe cross-section.	28
Fig. 11	Gap measurement.	28
Fig. 12	Picture of flow pattern facility.	29
Fig. 13	Picture of prototype test bed.	29
Fig. 14	Typical measured pressure profiles.	30
Fig. 15	Typical measured gap profiles.	30
Fig. 16a	Cardboard tube effect.	31
Fig. 16b	Water absorption effect.	31
Fig. 16c	Track support effect.	31
Fig. 17	Theoretical pressure distribution for assumed gap distribution qualitatively similar to measured distribution.	32
Fig. 18	Pressure source positions.	33
Fig. 19	Theoretical pressure distribution for uniform gap distribution.	34
Fig. 20	Theoretical pressure distribution for outer region gap distribution in which the gap increases with distance from the edge of the cavity.	35

Fig. 21	Oversized and undersized shoes.	36
Fig. 22a	Theoretical pressure distribution: sources within cavity.	37
Fig. 22b	Theoretical pressure distribution: sources outside cavity.	37
Fig. 23	Theoretical pressure distributions showing that sources within cavity control pressure there.	38
Fig. 24	Theoretical pressure distribution for one pressure source.	39
Fig. 25	Flow patterns obtained on flow pattern facility.	40
Fig. 26	Pressure profile for undersized shoe.	40
Fig. 27	Pressure profile for oversized shoe.	40
Fig. 28	Flow patterns obtained for aluminum track with standard feed hole pattern.	41
Fig. 29	Breakaway pressure versus driving weight.	43
Fig. 30	Feed hole patterns.	43
Fig. 31	Measured pressure distributions showing pitch stiffness.	44
Fig. 32	Scratch marks on shoes.	45

C_i	coefficients in finite element series solution
d	diameter of a feed hole
h	shoe-track gap
n	number of finite element nodes
$N_i(x, y)$	global shape functions
$P(x, y)$	pressure
$\tilde{P}(x, y)$	assumed pressure variation
$R(C_i, x, y)$	residual resulting from substitution of $\tilde{P}(x, y)$ into governing equation
S	bearing plane surface defined by x and y
$\bar{u}(x, y)$ $\bar{v}(x, y)$	mean velocities
$W_j(x, y)$	global weighting function
x y	global coordinate system
μ	laminar viscosity

Subscripts

i	shape function $N_i(x, y)$
j	weighting function $W_j(x, y)$

Abbreviations

LVDT	linear variable displacement transducer
MWR	methods of weighted residuals
TDC	Transportation Development Centre
UTIAS	University of Toronto, Institute for Aerospace Studies

1. INTRODUCTION

1.1 BACKGROUND

A division of the E. B. Eddy Forest Products Company of Canada, SailRail Enterprises, has, since the early 1970's, been developing a simple yet rugged air bearing device that has considerable potential for making major improvements in the way goods and materials are handled in certain transport systems. The development has been based largely on the ideas of Mr. H. E. Gladish, SailRail's General Manager, and has been assisted by, among others, the University of Toronto, Institute for Aerospace Studies (UTIAS). One of the authors of this report (P.A.S.) has provided technical advice since December, 1973 , [1] and has supervised the developmental testing done at UTIAS since 1975 [2] . More recently, UTIAS provided facilities and personnel for the installation of the system in the first two demonstration highway trailers. During the present Contract, the device was installed in a number of the E. B. Eddy warehouses, where it is now used on a routine basis for movement of goods into and out of highway trailers, with significant savings to the Company. Typically, an entire trailer load of pallets can be unloaded in less than 30 seconds; this contrasts with the time taken using fork-lift trucks, which may be as long as 45 minutes. However, although many tests of the practicality of the system have been passed, many basic technical questions important for future development and engineering optimization remain to be answered.

1.2 THE SAILRAIL CONCEPT

The SailRail system as currently implemented in a trailer-warehouse environment is shown in Figs. 1a and 1b. Two sets of guideways or "tracks" are built into the floor of the trailer and the warehouse to provide support and guidance for the two rows of pallets which comprise the typical trailer load. The two "rails" for each track are extruded from either a high density polymer plastic or aluminium. The plastic rails currently have a cross-section as shown in Fig. 2. They can be clearly seen in Fig. 1b, which is a photograph of the interior of the first development prototype trailer. The guideways also serve as manifolds to supply compressed air at about 750 to 1,000 mm Hg through a relatively small number of suitably spaced feed holes in the circular sector rail surface.

The guideways act as one of the two elements or mating surfaces for the bearing action. The other element, which is called the "shoe" and which is attached to the underside of the pallet, is approximately elliptical in cross-section as shown in Fig. 2. A key feature of the SailRail concept is the use of a combination of materials for the shoe which gives it a degree of compliance or flexibility. This eliminates certain mechanical alignment problems and plays a critical role in reducing the air flow rates required to effect an air bearing action.

At the current stage of development, the flexible element of each shoe, the so called "log", consists of creped* cellulose fibre tissue wound onto a

---

* Tissue artificially wrinkled during the manufacturing process by scraping tissue off the final drying drum.

3.8 cm diameter cardboard tube up to a diameter of about 13 cm; each log being about as long as a typical pallet, that is about 1.2 metres. The core and cellulose "filler" are inserted into a polyethylene tube ("cover") having a wall thickness of 1 mm or less and with a diameter chosen to obtain a close fit with the filler. The entire assembly is then flattened to form an approximately elliptic section with major and minor axes about 16.5 and 9.5 cm respectively. The ends of the tube are then usually sealed.

The air for bearing action is supplied through two sets of holes which are usually less than 0.75 mm in diameter and are spaced such that at any given time at least six are under a shoe. The holes are located on two generators parallel to the track axis, one at 15° from the centreline and one at 5° on the other side (the arrows in Fig. 3 show these locations). The feed holes are also inclined at an angle of about 20° to the tangent of the rail surface, and at 45° to the rail axis. This is shown in Fig. 3. The set of two rails comprising a track are installed so the 15° line of holes is on the outside and that the holes point towards the track centre. These features are characteristic of present SailRail designs; they contrast sharply with more conventional air bearing concepts, in which the nozzle axis is usually located centrally and along a radius. Intuitively, one would expect differences to depend critically on the magnitude of the feed hole diameter "d" relative to the local gap "h" between the shoe and track, as shown in Fig. 4.

One important feature of the shoe design is its demonstrated capacity for vibration isolation [3] . This has considerable practical significance for certain applications, one example of which is described briefly here. For some loads, such as paper goods shipped in cartons, the load actually carried is significantly less than trailer capacity, which is set either by weight or volume. This is because, if these loads are carried on conventional pallets, road induced vibration can cause the upper cartons to shift, which in turn greatly increases the time required to unload. When SailRail pallets are used, the trailer can be filled to volume capacity.

1.3 RELATIONSHIP TO EXISTING GAS BEARING CONCEPTS

The SailRail geometry is somewhat unconventional; however, in terms of gas bearing concepts, it appears to be an externally pressurized, restrictor stabilized, compliant surface thrust bearing [4 , 5] . The fundamental idea is illustrated in Fig. 5. The compliant surface deforms under the action of the hydrostatic pressure; the pressure gradients from feeding points to the outer boundaries or edges are in turn affected by the variation of the gap "h" between the compliant surface and the rigid mating surface. In the thrust bearing this has the effect of making the pressure nearly uniform except in the immediate vicinity of the edges. Figure 6, taken from the first development report to E. B. Eddy Forest Products, displays static pressure measurements taken under a prototype shoe. It is clear that significant fall-off in pressure occurs only for regions relatively close to the edge of the shoe; typically at points less than 12.7 mm (0.5") from the edge the pressure is still as high as 90% of values at the centre, so that the

edge is a very effective partial seal. In these tests the shoe construction differed considerably from that described previously; it consisted of a convex aluminum segment having the same cross-section radius as the track, onto which an approximately 12.7 mm (0.5") thick layer of tissue was held by a sheet of 0.1 mm (0.004") steel shim stock. The pressure measurements show that the prototype system did behave like a standard compliant surface device.

However the technical significance of a number of features of the design are unclear and perhaps even controversial. For example, one feature mentioned above is the use of inclined rather than radial air feed holes. It is possible that use of inclined holes might significantly reduce the hydrodynamic entry losses compared with those associated with radial holes. For example, if the diameter is very small compared to the local gap, so that $h/d \gg 1$, then jet entry losses would not be significantly affected by inclining the hole axis. However, if the hole diameter is very large compared to the local gap, so that $h/d \ll 1$, one would expect reduced entry losses because the hole would act as a settling or plenum chamber with an escape perimeter greater in the inclined hole case. When the present work started, values of h/d in the immediate vicinity of a feed hole were unknown.

The shoe construction also raises some basic questions. For example, it might seem that practical considerations would suggest the use of some filler material other than cellulose fibre. For example, a cast elastomer shoe might be simpler and cheaper to manufacture and less prone to degradation from exposure to wet environments. However, attempts to use other filler material have generally not met with success, but the reasons for this are not clear. One potentially important point to note is that the use of creped cellulose tissue introduces numerous small pockets of air in the filler, which makes the assembly very compressible; this contrasts with typical elastomers which are very incompressible. Another important characteristic of the material noted above is its capacity for vibration isolation. This leads to the speculation that the filler may be highly viscoelastic. It is also worth noting in this connection that the system has so far been found free of pneumatic hammer instabilities, a phenomenon that has been stated as a major difficulty in the application of more conventional compliant bearing concepts [4] .

It has also been suggested by the developer that the asymmetric location of the feed holes plays a significant role in generating the lateral restoring forces necessary for guidance and stability. However, no specific information which demonstrates this clearly was available at the beginning of the Contract.

1.4 OBJECTIVES OF THE PRESENT WORK

The overall objective of the project as described in the Work Statement of the Contract is to establish the operational characteristics of the system in terms of fundamental engineering concepts in fluid and structural dynamics. It is intended that the results should provide a basis for design optimization. Within this overall objective, certain specific tasks were identified at the

start of the Contract period. These were:

a) review of previous development work, in order to establish known facts about the system,

b) execution of exploratory experiments on a representative section of the track system in order to clarify observations made by the developer and confirm or extend these results,

c) definition of an experimental configuration which retains its principal characteristics and is amenable to mathematical analysis,

d) development of an analytical model which accounts for the resiliency and damping characteristics of the shoe material in order to predict its static and dynamic stability characteristics of the system.

The work statement also stipulated that possibilities for multimodal application be explored.

The review of data obtained prior to the present Contract (item a) provided many indications of the sensitivity of the concept to a wide variety of factors. However, all of this was taken on apparatus used for the development work. Many design changes were made as the testing proceeded, so that it was virtually impossible to interpret any of the results unequivocally. To quote but one example, prior attempts to compare the performance of systems with radial and inclined holes failed essentially because of lack of repeatability of the data. Hence development of a suitable prototype test bed (item b above) was seen as playing an important role in defining research priorities. This is described in Section 3.3.

The apparatus built for the work specified in item (c) above is described in Section 3.1. Its original purpose was to provide data on pressure and gap distributions between the shoe and the track to aid the theoretical development. The possibilities for theoretical analysis in relation to item (d) and a description of the analysis ultimately chosen are discussed in Section 2.1.

One item not specifically identified in the Work Statement, but which has proved to be of fundamental importance, was the development of methods for assessing the effectiveness with which air feed holes distributed the air under the shoe. Some simple flow visualization techniques were developed and the preliminary results obtained so far have provided valuable insights. The technique is described in Section 3.2.

It should be noted that a complete investigation of the SailRail concept's static and dynamic stability entails obtaining answers to several questions. The first question is to determine the mechanism by which the device generates vertical forces for lift, and obtains the required heave*

---

*The terms "heave, sway, pitch, roll and yaw" and "static and dynamic stability" are used in the same sense as in the literature on the dynamics of the motion of various vehicles, such as aircraft, automobiles and ships.

forces variation or "equivalent spring effect" for static* vertical stability. The next question is to ascertain the way in which the system generates the restoring forces and moments required for guidance and static stability. This includes investigation of sway, pitch and roll stiffness effects. The last question is the investigation of the dynamic stability of the motion. At the outset of the present work, the way in which the system generated lift, and static stability in heave and roll, seemed clear in qualitative terms at least. For example, the use of two shoes ensures that pressure differentials for restoring moments in roll can be established under the pallet.

The basic question in relation to pitch stiffness is: To what extent are the restoring forces and moments required for static stability in pitch generated by direct shoe-rail contact as opposed to redistribution of pressure associated with the air bearing action? It has already been noted that the Developer has suggested that the asymmetric hole locations provide for lateral restoring force, but no data of any kind was available. Consequently, an attempt to provide some insight into this question has been made.

Finally it is noted that the very low speeds involved in the present applications indicate that dynamic stability phenomena should not present problems. One potential exception to this is the phenomenon of pneumatic hammer. This has been observed only once during the development testing, when very high loads were used.

2.1 DISCUSSIONS OF THE POSSIBILITIES FOR ANALYSES

Computation of compliant surface gas bearing characteristics presents a number of difficulties. A complete analysis requires a formulation describing both the fluid mechanical processes and the structural deformation of the compliant element under the action of a pressure distribution, which is determined by the fluid mechanics. The equations for these two aspects are coupled and have to be solved simultaneously. Even in the simplest possible case, a thrust bearing having axial symmetry and in which the fluid flow processes involved can be described by ordinary differential equations; these equations are nonlinear and have to be solved numerically. A major complication is the characterization of the material properties of the compliant element. Calculations to date have generally been limited to consideration of a column model of the compliant material; this assumes that the local compression is proportional to the local hydrostatic pressure, and that there is no shearing interaction between adjacent parts of the compliant element. This is in spite of the fact that elastomers are highly incompressible.

The SailRail geometry is very complex, both the irregular layout of the air feed holes and the geometry and construction of the shoes effectively rule out the possibility of a simple analysis. The fluid flow processes are also complex. The air supply pressure is typically of the order of 1000 mm Hg and the pressure in the shoe near a feed hole may be about 300 mm Hg. With these pressures and for typical air flow rates, the Reynolds number based on hole diameters is about 10,000. Thus the flow through the feed hole and in its immediate vicinity is compressible, turbulent and quite possibly choked. However, owing to the spreading out of the flow into the cavity under the shoe, the flow appears to rapidly relaminarize and indeed effectively comes almost completely to rest.

Computation of the shoe structural deformation also presents difficulties. The effective constituitive properties of the shoe material are not available. Furthermore some evidence available from the development work suggests that deformation of the entire elliptical section might have to be incorporated.

For the present contract, the compromise described below was adopted. A finite element hydrostatic lubrication analysis of the air flow processes occurring in the small gap separating the shoe and track was performed [6]. For the analysis it was assumed that the flow could be modelled by the compressible Reynolds equation for pressure and that the feed holes could be modelled as pressure sources. Also, no attempt was made to determine structural deformations. Instead, specific gap distributions qualitatively similar to measured distributions were assumed, and the corresponding pressure distributions were calculated. The finite element analysis is described in detail in Appendix A and briefly in Section 2.2. The measured gap distributions were obtained using the facility described in Section 3.1. To deal with feed holes in more detail one could try locally a finite difference procedure similar to that developed by Launder et al [7] for simple thrust bearings. This was attempted here but without success, mainly because of numerical stability and convergence problems when applied to the SailRail geometry.

Consideration was given to several other lines of approach. One was to model a two dimensional slice of the entire system. It was envisaged that the feed orifice would be modelled as a slot, and the flow between shoe and track treated as one-dimensional. It is feasible, in principle at least, to incorporate a numerical simulation of the structural deformation of the entire shoe for this case. However development of this approach was not emphasized mainly because the one dimensional fluid flow model may be totally unrepresentative of the flow processes involved.

2.2 BRIEF DESCRIPTION OF THE FINITE ELEMENT ANALYSIS

Essentially, the finite element method is a technique for obtaining approximate solutions to differential equations for which analytical solutions are either not possible or very tedious to obtain. It is used here because of the irregular feed hole spacing and also because of nonlinearities in the governing differential equation. It is just one of a number of methods contained in the Methods of Weighted Residuals (MWR) [8], and it is similar to finite difference methods [9] in that it replaces the governing differential equation by a system of algebraic equations, the solution of which satisfies approximately the governing equation.

The governing equation here is the compressible Reynolds equation for pressure (see Figure 7 and Appendix A for derivation):

$$\nabla \cdot (ph^3 \nabla p) = 0 \tag{2.1}$$

where

$$\nabla = \frac{\partial}{\partial x} i + \frac{\partial}{\partial y} j \tag{2.2}$$

and p is the absolute static pressure and h is the gap height. Equation (2.1) expresses a direct balance of viscous and pressure forces in the plane of the bearing with the assumptions that there is no forward or heave motion and that the surfaces are rigid and nonporous and the spacing between them is very small. Note the h^3 term in the governing equation. Note also that because of compressibility the governing equation is nonlinear. These two factors complicate the solution algorithm.

One seeks by the finite element method an approximate solution to Reynolds equation of the form

$$\tilde{P}(x, y) = \sum_{i=1}^{n} C_i N_i(x, y) \tag{2.3}$$

where the functions $N_i(x, y)$ are members of a complete set of specified functions. The coefficients C_i are chosen in such a way that when (2.3) is substituted into (2.1) it satisfies it in some average sense over the entire solution domain. This is done by making the resulting residual orthogonal

to members of the complete set of functions $N_i(x, y)$ by writing

$$\int_S N_j(x, y)R(C_i, x, y)dxdy = 0 \qquad j = 1, \ldots, n \tag{2.4}$$

The details of this as mentioned are given in Appendix A. When evaluated, the weighted integral expressions give a system of algebraic equations for the coefficients C_i, which in a finite element analysis are actually the pressures at specific positions called nodes throughout the solution domain. Boundary conditions are applied in the usual way and a solution to the final algebraic equation system is obtained using a Gauss-Seidel iteration [8, 9].

For a very long shoe-track configuration fed by a longitudinal slot source, the problem becomes one dimensional and some simple analytic solutions can be obtained. One of these is outlined in Appendix B.

3.1 GAP MEASUREMENT FACILITY

This facility was designed to obtain typical distributions of gap between the shoe and the track, especially in the immediate vicinity of a feed hole where it could possibly explain performance differences between inclined and radial holes. The facility is shown schematically in Figure 8 and pictorially in Figure 9. Its dimensions are given in Table 1. The shoe being tested rests on a steel H beam support structure. A typical track, with three rows of probes, sits on top of the shoe. The cross-section of a typical probe is shown in Figure 10. The probe is simply a steel tube which is attached rigidly into the lower surface of the track by using epoxy cement. The region where the tube passes through the upper surface is sealed by using a flexible silicone sealant. The latter helps minimize bending of the tube when the track is pressurized.

Table 1. Dimensions of Gap Measurement Facility

Shoe Log	86 cm long 14.5 cm diameter
Shoe Cover	high density polyethylene 0.75 mm thick
Feed Holes Pairs	inclined 17.75 cm spacing 0.70 mm diameter
Track	plastic 15.7 cm ± 0.2 cm radius
Nominal Weight	450 kg
Nominal Track Pressure	1000 mm Hg

The probe can be used for measuring either pressure or gap. For gap measurement, a small steel rod of diameter slightly less than the inside diameter of the tube is inserted as shown in Figure 11. A Schaevitz Linear Variable Displacement Transducer or LVDT is used to measure the height that the rod extends above the upper surface of the tube. The gap is simply the difference between the height measured when the track is not pressurized and the height measured when the track is pressurized. For pressure measurements, a Heise gauge capable of reading static pressures up to 2500 mm Hg above atmospheric is used. Overhanging weights are used to load the shoe.

3.2 FLOW PATTERN FACILITY

This facility was designed to obtain air flow patterns in the gap separating the shoe and the track. The facility is shown pictorially in Figure 12. Its dimensions are given in Table 2. As with the gap measurement facility, the shoe being tested rests on a steel H beam support structure;

a clear plexiglass track sits on top of the shoe. Each feed hole in this track is fed separately. A loading mechanism designed to give as uniform a loading as possible without interfering with the flow pattern visualization sits on top of the track. Clamps attached to the loading mechanism are used to load the shoe.

Table 2. Dimensions of Flow Pattern Facility

Overall Length	102 cm
Test Sections (Windows)	15.24 cm wide 20.32 cm long
Plexiglass Track	12.7 cm radius
Feed Hole Pairs	30.5 cm spacing
Feed Holes Inclined and Separately Fed	

Various flow pattern visualization techniques were employed. Initially, the aim was to introduce smoke into the air supply line which would be carried by the air flow into the shoe-track gap. An oil smoke generator was constructed and installed. However, it proved to be inadequate mainly because the smoke condensed back to liquid oil at the holes. Chemicals such as titanium tetrachloride capable of reacting with moisture in the supply air to form smoke were ruled out because of possible toxic, corrosive and other effects.

One technique which provided some insight used liquid crystal mylar sheets attached to the plastic shoe cover. The colour of a liquid crystal sheet is temperature dependent and sheets usually respond only in a given temperature range. At the lower temperature they are usually black while at the higher temperature they are usually dark blue. The sheets chosen for the flow pattern experiments had temperature ranges which excluded typical ambient temperature. To visualize the flow pattern, the supply air was either heated or cooled depending on the temperature range of the particular sheet used.

The most promising technique used ammonia sensitive sheets attached to the plastic shoe cover. Ammonia vapor was introduced into the supply air by passing the air through the top part of a metal container with liquid ammonia at the bottom. When the air-ammonia gas mixture entered the shoe-track gap, the ammonia caused the sheets to change colour locally.

To aid in the interpretation of the flow patterns, the plexiglass track was fitted with pressure probes.

3.3 PROTOTYPE TEST BED

Figure 13 is a photograph of this facility; its dimensions are given

in Table 3. The only major difference between this facility and the configuration used in practice is that the rails are supported continuously instead of at discrete points about 0.3m apart. It was believed that the uneven support used in earlier facilities was a major factor in causing lack of repeatability of the measurements. As can be seen, the facility consists of two long steel H beams connected transversely by five shorter H beams. The two long beams are used to provide even track support. The H beam structure rests on four heavy duty jacks. These are used to level the support surface longitudinally.

Table 3. Dimensions of Prototype Test Bed

Longitudinal H Beams	304.8 cm long	25.4 cm deep 1.27 cm thick
Traverse H Beams	58.4 cm long	25.4 cm wide
Pallet	121.9 cm long 101.6 cm wide	
Shoe	120 cm long approx.	
Feed Hole Pairs	30.5 cm spacing	
Track	15.3 cm radius	

It was decided to use as a performance index the equivalent air flow power required to start motion of a loaded test pallet under the action of a known driving force. The rationale for using breakaway power as a performance index was to keep the number of parameters to be controlled to a minimum; the use of breakaway power removed the details of the forward motion which ultimately resulted.

4. RESULTS

4.1 MEASURED GAP AND PRESSURE PROFILES

Figure 14 gives the average of transverse pressure profiles obtained for 4 nominally identical shoes. The vertical bar through each data point in the top graph indicates the maximum and minimum readings recorded for that point. It shows that readings are subject to greater scatter at the left hand side. This could be due to the holes being angled away from the left side. It could also be an indication of a slightly asymmetric load. Note that the average profiles for the two transverse sections are almost identical and that the pressure is uniform centrally with an approximately linear fall off along the sides of the track. Note also that the system is not operating at optimum as the uniform pressure region occupies approximately only half of the possible support area.

Figure 15 gives the transverse gap profiles for one of the shoes of the previous figure. Here one can see a central cavity region which correlates well with the uniform pressure region in Figure 14; in other words, behaviour very similar to conventional compliant surface devices. If one assumes that the transverse profiles are the same at every longitudinal position then the mean longitudinal flow would be zero and the transverse flow per foot of track in cfm would be given by (see Appendix A)

$$Q_T = \left(- \frac{h^3}{12\mu} \frac{dp}{dx} \right) 2 \times 60 \qquad (4.1)$$

$$= \frac{-10h^3}{\mu} \frac{dp}{dx}$$

The data in Figures 14 and 15 puts Q_T in the range 0.1 cfm to 1.0 cfm. The flows observed in practice are approximately of this order.

Values of h/d in the immediate vicinity of a feed hole were found to be typically of the order of 1/5 (see Figure 15). As mentioned previously this could explain the sometimes observed performance difference between radial and inclined holes. Recall that one would expect a difference for $h/d \ll 1$ (see Section 1.3).

The pressure profiles presented in Figure 16 show how critical the log's flexibility is to system performance. For example, Figure 16a shows that when the cardboard tube is removed the pressure profiles can be very erratic. For this experiment, the shoe was shaped into its elliptic form before the cardboard tube was removed. When the tube was removed, some tissue had to be removed along with it. This could not be made uniform along the length of the shoe, which could explain why profiles are so different for the two transverse sections. Figure 16b shows that tissue water absorption can give transverse pressure profiles which are flat right to the transverse edges of the shoe. Presumably, this is due to the tissue when wet forming a seal at these edges. Figure 16c shows that allowing the track to deflect by supporting it only at its longitudinal ends (see Figure

8b) can cause a large drop in pressure at the deflected section. With the end supports the track deflected at midspan approximately 6.35 mm (1/4"). The end supports were 7 cm wide, 18 cm long, and 6.35 mm thick.

4.2 QUALITATIVE COMPARISONS WITH THEORETICAL PRESSURE PROFILES FOR SPECIFIC GAP DISTRIBUTIONS

Typical theoretical results obtained are shown in Figure 17. The calculated pressure distribution is given in the upper left hand corner of the figure. Directly beneath it is the assumed gap distribution. Selected transverse profiles are given in the plots on the right hand side. For the results, pressure sources were placed at the positions marked "•" in Figure 18. The assumed gap distribution was qualitatively as measured. At the periphery of the shoe the pressure was taken to be atmospheric while at each of the source boundaries it was taken to be 1.5 times atmospheric, the latter being a typical measured shoe pressure. As can be seen, the pressure profiles obtained are qualitatively similar to those measured. In particular the profiles are flat within the cavity region, and there is a linear fall-off in the outer regions.*

Figure 19 shows the extremely poor pressure distribution obtained by assuming a uniform gap throughout. Again the presentation format is as in Figure 17. On comparing Figures 17 and 19, one can see why in practice the shoe flexibility has been found to be so critical; it is shoe flexibility which determines to a large extent the gap distribution.

The computer programme was used to study a number of other configurations. For example, Figure 20 shows the pressure profiles obtained for a gap distribution with a cavity region the same as in Figure 17 but with an outer region in which the gap increased with distance from the edge of the cavity. The main difference between these profiles and those presented in Figure 17 is the pressure is zero in the outer region whereas in Figure 17 there is a linear fall-off from the cavity to the edge of the shoe. It will be shown that the results in Figure 20 correspond approximately to an undersized shoe while those in Figure 17 correspond to an oversized shoe (see Figure 21). Figure 22 compares the pressure distribution obtained for the case where the sources are within the cavity to that obtained for the case where the sources are outside. The gap distribution for each case was as in the previous figure. One can see that having the sources outside the cavity gives a very poor pressure distribution. Figure 23 shows that the source within the cavity controls the pressure there. The source just outside the cavity has virtually no effect. Figure 24 shows that just one source within the cavity gives a reasonable pressure distribution.

4.3 FLOW PATTERNS

Typical results obtained using ammonia sensitive sheets on shoes in the flow pattern facility are shown in Figure 25. The picture on the left was

---

*The results were not very sensitive to the geometric size of the pressure sources.

obtained using blueprint paper while the picture in the middle was obtained using an ammonia sensitive mylar film. Both were obtained using an undersized shoe while the picture on the right was obtained using mylar film and an oversized shoe (see Figure 21). Figure 26 gives a pressure profile for the undersized shoe case. It shows that the dark region on the film contains the uniform pressure region which as shown in the previous section in turn contains the cavity. Note the similarity of the pressure profile to the theoretical profiles given in Figure 20. Figure 27 gives a pressure profile for the oversized shoe case.

An important feature of the ammonia sensitive sheet technique is that it can be used in the prototype test bed. All one has to do is introduce the ammonia-air gas mixture into the track being used and use shoes with ammonia sensitive sheets attached. Typical results obtained for an aluminum track with the standard pattern of inclined feed holes are shown in Figure 28. These results have not been interpreted fully, and the technique itself still requires refinements. However, the following points are apparent:

a) a significant amount of air from the feed holes furthest from the centreline of the track is leaking out locally to atmosphere; this suggests that the present position of these holes is not optimum.

b) results are different for different exposure times. However, for a given exposure time, results are approximately repeatable;

c) for high track pressures longitudinal coloured regions somewhat similar to those shown in Figure 25 occur; in Figure 25 these regions were shown to correlate well with a central cavity.

4.4 INITIAL RESULTS FROM PROTOTYPE TEST BED

Although the data obtained from this facility to date is very limited, some trends have been observed. For example, six sets of shoes were tested on plastic tracks with the standard pattern of feed holes (see Figure 3 and Table 3). For the tests the holes were inclined, the load was 1023 Kg, and the driving weight was 50 Kg. The shoes were found to give the same breakaway pressure to within approximately 10%. Also, some tests on aluminum tracks indicated almost the same performance as on the plastic tracks. Hence the lack of repeatability in the development work done prior to the Contract is believed to have been due mainly to uneven track support.

A breakaway pressure versus driving weight curve obtained for one set of shoes is shown in Figure 29. For this the load was 1023 Kg and the tracks were plastic with the standard pattern of inclined feed holes. One can see that the relationship is almost linear. The small amount of scatter for each driving weight was found to be due partly to starting at different positions along the track.

The standard pattern of feed holes was compared with the pattern shown in Figure 30. In each case, the tracks were aluminum, the load was 1023 Kg,

the holes were inclined, and the driving weight was 51 Kg. It was found that the breakaway pressure for the new arrangement was only 93% of that for the standard arrangement. Also, there was much less hesitation after breakaway with the new arrangement. This suggests that one cannot ignore the details of the motion which ultimately results. Thus dynamic testing is required and the performance index is in need of some refinement. It was observed in more recent tests done at UTIAS and at SailRail Enterprises that when aluminum tracks are used there is often a tendency for performance to degrade due to the shoe cover picking up small chips of aluminum apparently scraped from the tracks themselves. These chips roughen up the cover surface and cause a large increase in shoe-track contact friction. However, for the above tests, the results were reasonably repeatable from one trial to the next which suggests that for these tests the effect was not large.

The performance of inclined feed holes was compared with that of radial feed holes. For the tests, the same set of aluminum tracks was used. The load was 1023 Kg and the driving weight was 51 Kg. To ensure no effect due to aluminum chips being ingested into the shoe cover, the same log was used but the plastic cover was changed between tests. When spaced in the standard pattern, the breakaway pressure for the radial hole case was found to be approximately 95% of the inclined hole value; however, the total track flow was higher at 127% of the inclined value and the power index (Track Pressure x Total Flow) was 121%. Thus inclined holes are marginally better from a power standpoint.

The standard pattern of radial holes was also compared with a pattern in which radial holes were spaced centrally as shown in Figure 30. In this case the breakaway pressure for the new pattern was only 84% of that obtained with the standard pattern.

4.5 DISCUSSION

One interesting observation made during tests on the flow pattern facility is that the width of the uniform pressure region is approximately the same for both oversized and undersized shoes and is 6.25 ± 1.25 cm (see Figures 26 and 27). The cardboard tube inside the shoe when flattened is approximately 6.25 cm. This suggests that the sealing action results from a concentration of material at the tips of the crushed cardboard tube (see Figure 2). If this hypothesis is verified, it could provide a basis for shoe design.

It was also observed during tests on the flow pattern facility that the system obtains its pitch stability from a shift in the centre of the shoe pressure force and not from shoe-track contact (see Figure 31). This was demonstrated with the plexiglass track suitably instrumented with pressure probes and with load cells installed in the clamping devices; some detailed calculations are given in Appendix C.

5. CONCLUSIONS AND SUGGESTIONS FOR FUTURE WORK

5.1 CONCLUSIONS

The good qualitative agreement obtained between the pressure distributions measured under the shoe, and those computed by applying the Reynolds equation for hydrostatic lubrication to the measured gap distribution, have confirmed that the SailRail system is a type of compliant air bearing device, but it has a number of distinctive features. The calculations also show that it is useful to consider the fluid mechanical processes involved as passing through three distinct phases, each in separate regions under the shoe. The first occurs in the immediate neighbourhood of the feed holes. The flow emerging from these holes is turbulent, compressible, and may be choked. Furthermore, because the local gap may be as little as 1/5 of the feed hole diameter, and because the holes are inclined to the track surface, the geometry is complex. Consequently the details of the flow in this region cannot be readily characterized in terms of known data. As the feed air spreads out under the shoe it slows down and, in a distance which may be as little as 1 cm, reaches a point where fluid flow forces are very small, even negligible. The fluid is effectively at rest and the pressure is constant; hence one may call this the cavity region. It occupies most of the pressurized or "footprint" area under the shoe. The air escapes from under the shoe in what is called the seal region; this occupies a strip around the periphery of the pressurized area which is 2 to 4 cm wide.

The measured pressure distributions show that the pressurized support area is only about 7 cm wide, very much less than the width of the shoe. Furthermore, observations of scratch marks appearing on shoes that have been used both in the prototype test bed at UTIAS (Figure 32a) and in the E. B. Eddy warehouses (Figure 32b) indicate that the seal region itself may occupy approximately 50% of the possible footprint area. It is suggested that the location of the sealing region is determined mainly by a concentration of the cellulose filler material in the neighbourhood of the tips of the flattened cardboard tube that forms the core. Hence one very important conclusion is that the shoe should be redesigned to increase the width of the cavity region. One should be able to obtain a large increased load capacity with virtually no increase in the air flow rates required, or greatly reduce the air flow rates at existing load capacities. The latter change would also greatly reduce the track manifold pressure required and hence the air lost directly to atmosphere on the uncovered portions of track in the typical installation. It is possible that the shoe may only have to be modified very simply to obtain this improvement; for example, if the location of the seal region is determined by the size of the flattened core, then simply increasing the diameter of the core tube might achieve this end.

Measurements of system performance on the prototype test bed have shown that the main difficulty encountered in early development testing, namely lack of repeatability of data, was due to the use of discrete rather than continuous support of the track. Tests on a representative sample of shoes showed good reproducibility within the sample, and no significant difference in performance was observed when the track material was changed from plastic to aluminum. Tests comparing the performance obtained with the use of radial and inclined feed holes suggest that the inclination of the holes has at most a minor effect.

It appears that radial feed holes give slightly better performance, but the data obtained was insufficient to draw a clear-cut conclusion. Tests comparing performance of the highly asymmetric standard feed hole arrangement with a modified arrangement, in which all feed holes were located nearer the centre and distributed more uniformly, indicated an improved performance for the latter.

However, the most important information about the hole layout was obtained from the flow visualization tests. These convincingly show that most or all of the air fed into the set of holes located on the 15° or outer generator does not enter the cavity region but escapes locally to atmosphere. This occurs because these holes appear to be located in the sealing region and, although the orientation of these inclined holes is such as to direct the air towards the cavity region, they have little or no effect toward this goal. Both these results and those obtained on the prototype test bed therefore suggest that, for the generation of lift forces, the layout and orientation of the feed holes is not optimum.

Only a very limited amount of information on the stability aspects of this system was obtained. However the measurements described in Appendix C strongly suggest that the restoring moments required for pitch stability are generated mainly by changes in the pressure distribution under the shoe and not by forces arising from shoe-track contact. This is an important finding, since it suggests that the forces required for lateral stability and guidance might also be generated by changes in the pressure distribution. Specifically it requires that the externally applied lateral force move the shoe until the footprint is shifted laterally to a region on the track surface where the resolved horizontal component of the force generated by the pressure distribution is sufficient to balance this externally applied force. It is possible that, in this situation, the 15° row of feed holes is now well inside the cushion seal region. However this idea had yet to be tested experimentally.

5.2 SUGGESTIONS FOR FUTURE WORK

Considerably more work on the prototype test bed is required to establish unequivocally the sensitivity of the performance of the SailRail device to the many parameters suggested by the Developer as being of practical significance. Some minor improvements in technique for determining the track-pressure corresponding to lift-off and for flow visualization procedures, but apart from this, a considerable amount of data can be accumulated quickly. Furthermore, although this is an empirical approach, the authors regard it as playing a key part in supporting the Developer's own programme. However, its most important function will be to assist in establishing research priorities. Two examples of the way in which this is expected to help are noted here. Development work undertaken prior to the present Contract indicated that the shoe cover might have an optimum thickness for best system performance. Owing to time and effort limitations, this point was not addressed in the present programme. Yet, if the existence of such an optimum is established, it would have important implications for any further theoretical analysis for reasons discussed below. The test bed can also quickly provide answers to such questions as the effect of the size of the core on the width of the cavity region.

Both of these tests are examples of those required for investigation of the most important aspect not treated to date, namely the structural deformation of the shoe and the way in which it interacts with the pressure distribution generated by the fluid mechanics. Owing to the complex geometry of the shoe, considerable physical insight may be required before a suitable model can be defined. For example, the simplest possible model for this interaction process is the column-spring model used in the analysis of compliant air bearings and mentioned earlier. Yet such a model would not account for any bending stiffness effects that might be introduced by the shoe cover and which might play a role in determining the shape and size of the cavity region. If the test mentioned above indicated that an optimum cover thickness existed, then the presence of significant bending stiffness effects is indicated. Also, to facilitate comparison of theory and experiment, a simplified shoe geometry might have to be defined. It has been suggested that such a geometry might be a uniformly thick layer of tissue attached to the curved part of a rigid segment. In any case, suitable tests for determining the local stiffness characteristics of the tissue have to be developed; this item should be given high priority.

Considerable work on the fluid mechanical aspects of the device is also required. The finite element analysis and the experiments have shown that this work may be conveniently broken into two parts. The first is investigation of the flow in the feed hole region, and the second is analysis of the air escape process in the seal region. For both tasks, theoretical analyses and special experiments appear to be required. For analysis of the flow in the feed-hole region, the Teach-T finite difference algorithm for the computation of turbulent flows developed by Gosman et al [10] might be suitable. Experiments on a suitably instrumented scaled up model are also required. It is envisaged that, at the very least, such experiments will provide empirical data on pressure changes due to entry losses.

For the analysis of the fluid mechanics in the seal region, advantage can be taken of the fact that the flow is laminar, and possibly inertialess. Furthermore, almost all of the air escapes along the sides of the shoe, so that the flow should be two dimensional. Also, since the gap in the seal region $h = h(x)$ is slowly varying, the flow may be similar in many respects to a boundary layer. Some preliminary steps in this direction have already been taken; one example is described in the report. The analysis would, ultimately, have to include the local structural deformation of the shoe, but initially development could proceed by using a specified gap distribution obtained from experiment. It is noted that detailed accurate profiles of gap distribution in the seal region have yet to be obtained. It appears that the technique used in the present work may not have sufficient resolution so that an alternative method may have to be found.

Finally, it is noted that vibration of the shoe cover in the neighbourhood of the nozzle regions might, under some circumstances, occur and this could have a significant effect on flow processes there. The speculation is that flow limitation similar to that which occurs in flexible tubes, and analogous to the gasdynamic choking of the compressible flow in a convergent-divergent nozzle could be present near the holes. Some preliminary calculations of the relevant

wave speed c, given by

$$c = \sqrt{\frac{h}{\rho}\frac{dp}{dh}} \qquad (5.1)$$

indicate that flow speeds probably exceed this near the holes. In experiments at UTIAS on this process, it has been noted that this type of choking is often associated with tube vibrations.

1. Sullivan, P. A., "An Evaluation of an Air Cushion Suspension Device Known as Sailstrip or Sailrail", Aerospace Engineering and Research Consultants Ltd., Toronto, Report No. 73-12, December 1973.

2. Sullivan, P. A., Parravano, G. J., "Results of an Experimental Evaluation of an Air Support Device Known as Sailrail", Aerospace Engineering and Research Consultants Ltd., Toronto, Report No. 75-04-2, January 1976.

3. Davidge, R. O. C., "Evaluation of the Vibration Isolation Characteristics of SailRail Air Cushion Pads", Department of National Defence, Quality Engineering Test Establishment, March 1980.

4. Lowe, I., "Some Experimental Results from Compliant Air Lubricated Thrust Bearings", Transactions of the ASME: Journal for Lubrication Technology, October 1974, pp. 547-560.

5. Benjamin, M., Castelli, V., "A Theoretical Investigation of Compliant Surface Journal Bearings", Transactions of the ASME: Journal of Lubrication Technology, January 1971, pp. 191-201.

6. Streeter, V., "Handbook of Fluid Dynamics: Section 22, Lubrication Mechanics", McGraw-Hill, 1961.

7. Launder, B. E., Leschziner, M. A., "Flow in Finite-Width Thrust Bearings Including Inertial Effects: I-Laminar Flow; II-Turbulent Flow", ASME Journal of Lubrication Technology, Vol. 100, July 1978.

8. Finlayson, B., "The Method of Weighted Residuals and Variational Principles", Academic Press, 1972.

9. Roache, P., "Computational Fluid Dynamics", Hermosa Publishers, 1972.

10. Gosman, A., Ideriah, F., "Teach-T: A General Computer Program for Two Dimensional, Turbulent, Recirculating Flow", Dept. of Mechanical Engineering, Imperial College, London, England, 1976.

FIG. 1a TRAILER-WAREHOUSE SYSTEM

FIG. 1b TRAILER INTERIOR

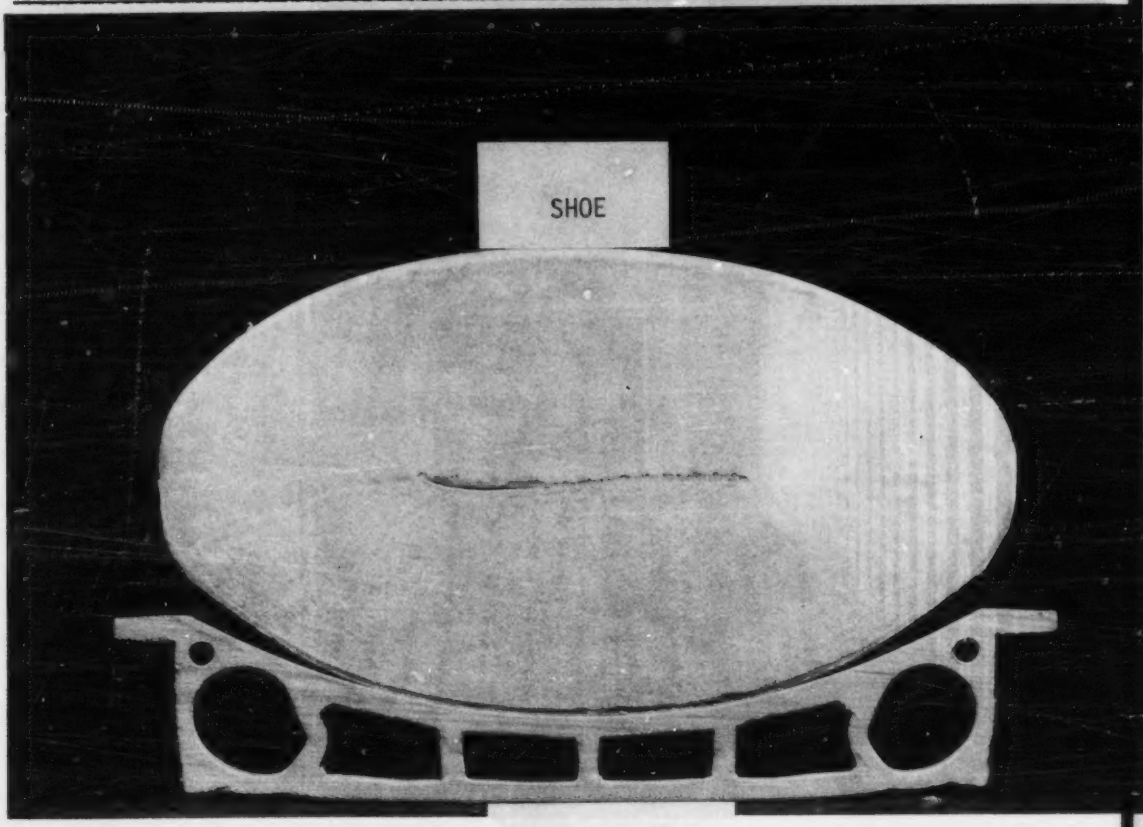

FIG. 2 CROSS-SECTION OF TRACK AND SHOE

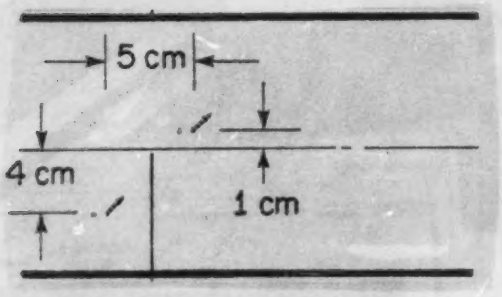

FIG. 3 STANDARD FEED HOLE PATTERN

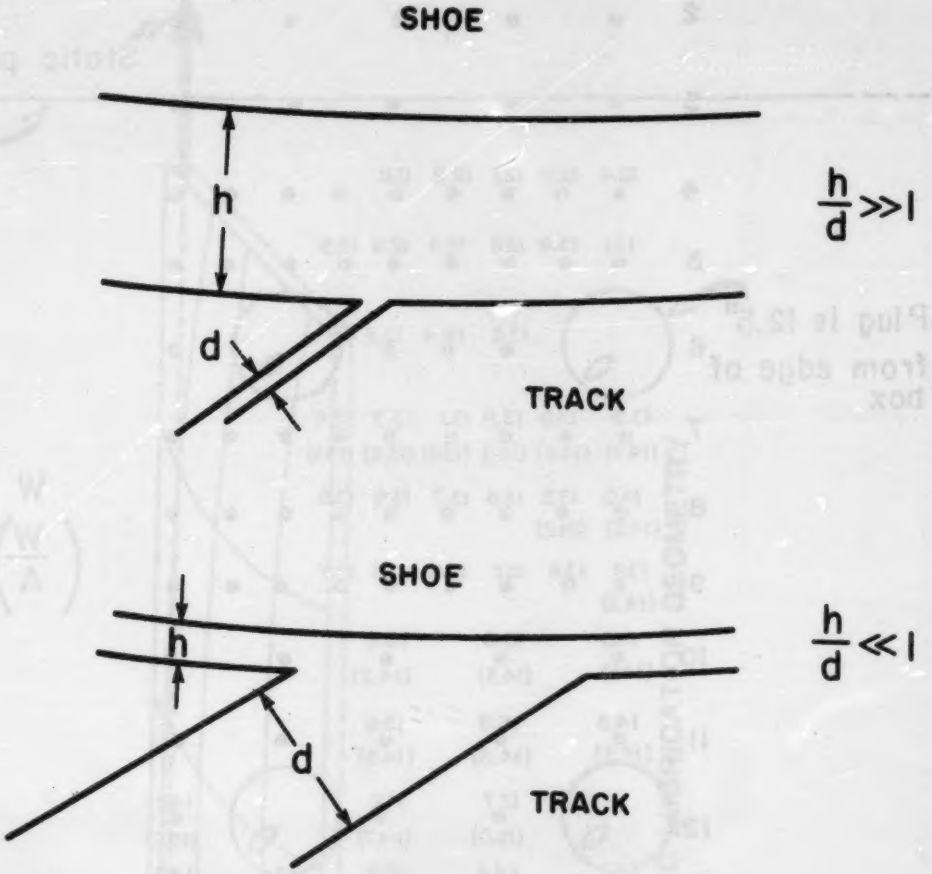

FIG. 4 POSSIBLE GAP FEED HOLE CONFIGURATIONS

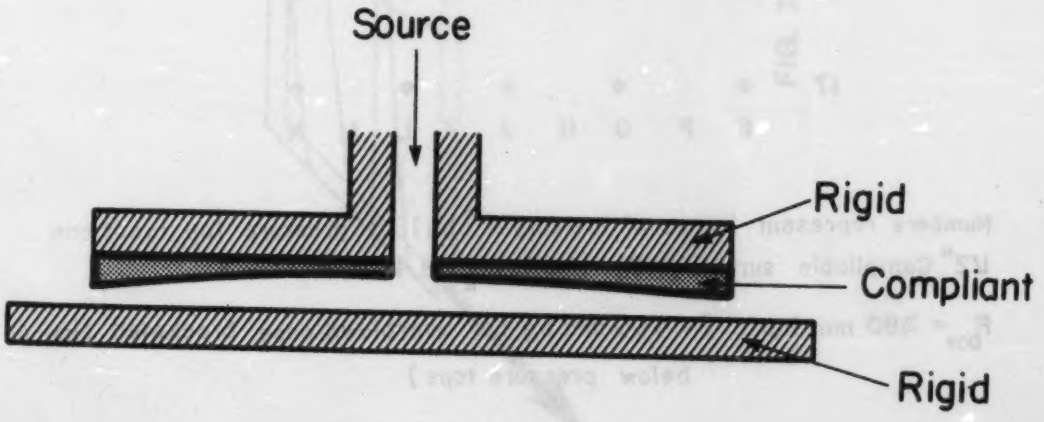

FIG. 5 COMPLIANT SURFACE AIR BEARING

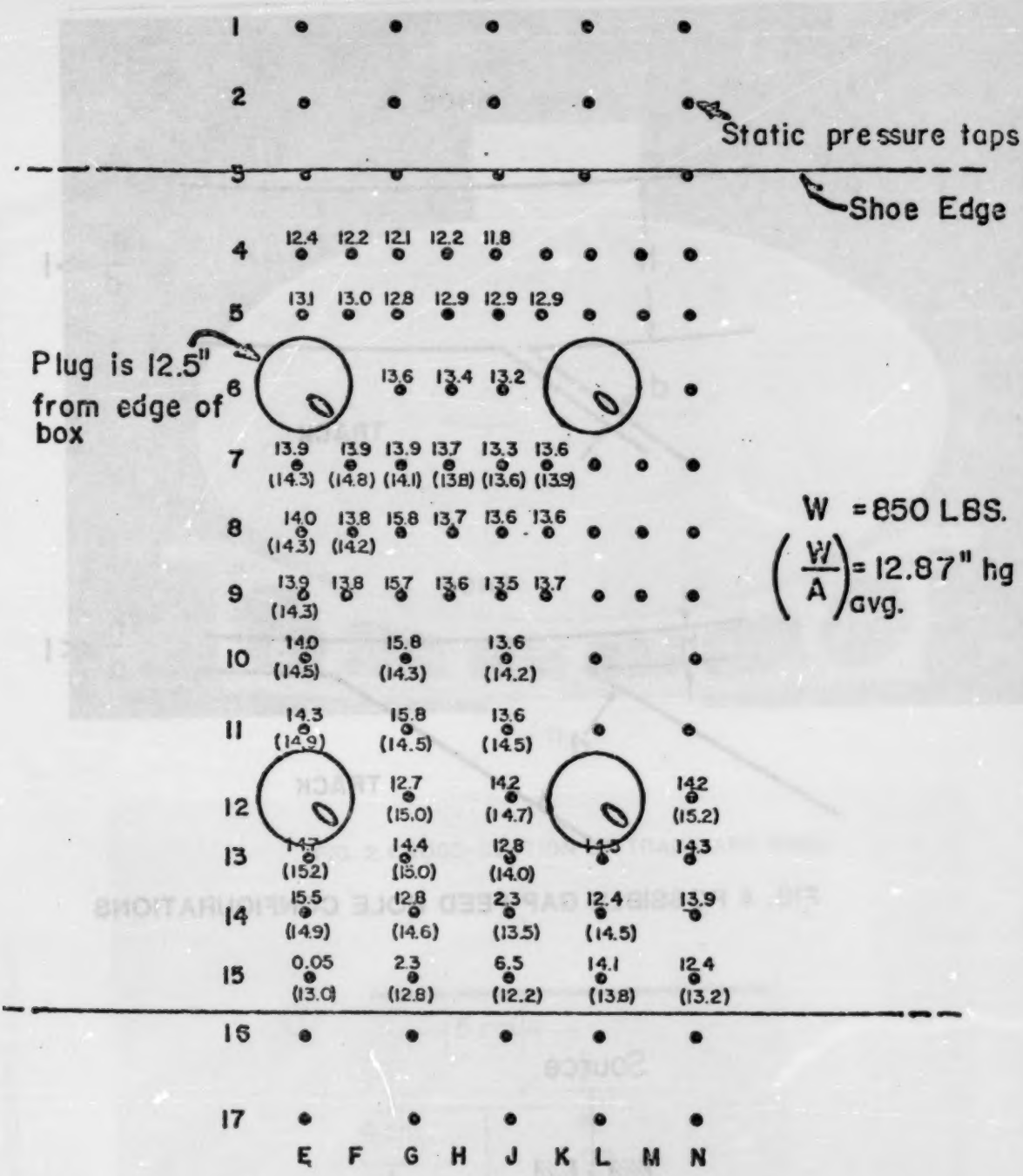

Numbers represent inches of mercury (" hg) at pressure tap locations

1/2" Compliable surface, $\alpha_1 = 11.6°$, $\alpha_2 = 8.4°$

P_{box} = 380 mm. hg. (= 400 mm. hg. for overblown case, bracketed figures below pressure taps)

FIG. 6 PROTOTYPE SHOE PRESSURE DISTRIBUTION

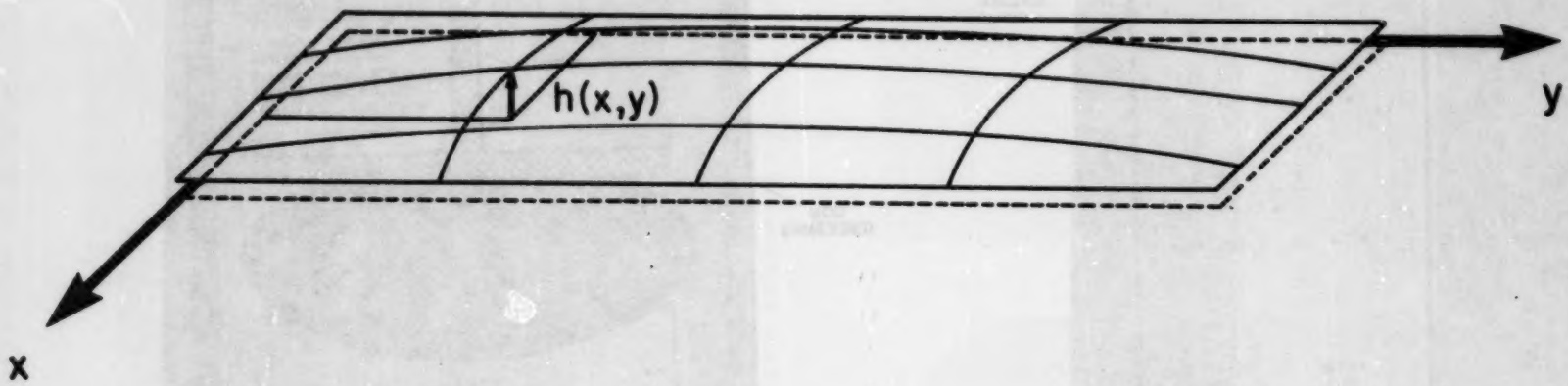

FIG. 7 HYDROSTATIC LUBRICATION GEOMETRY

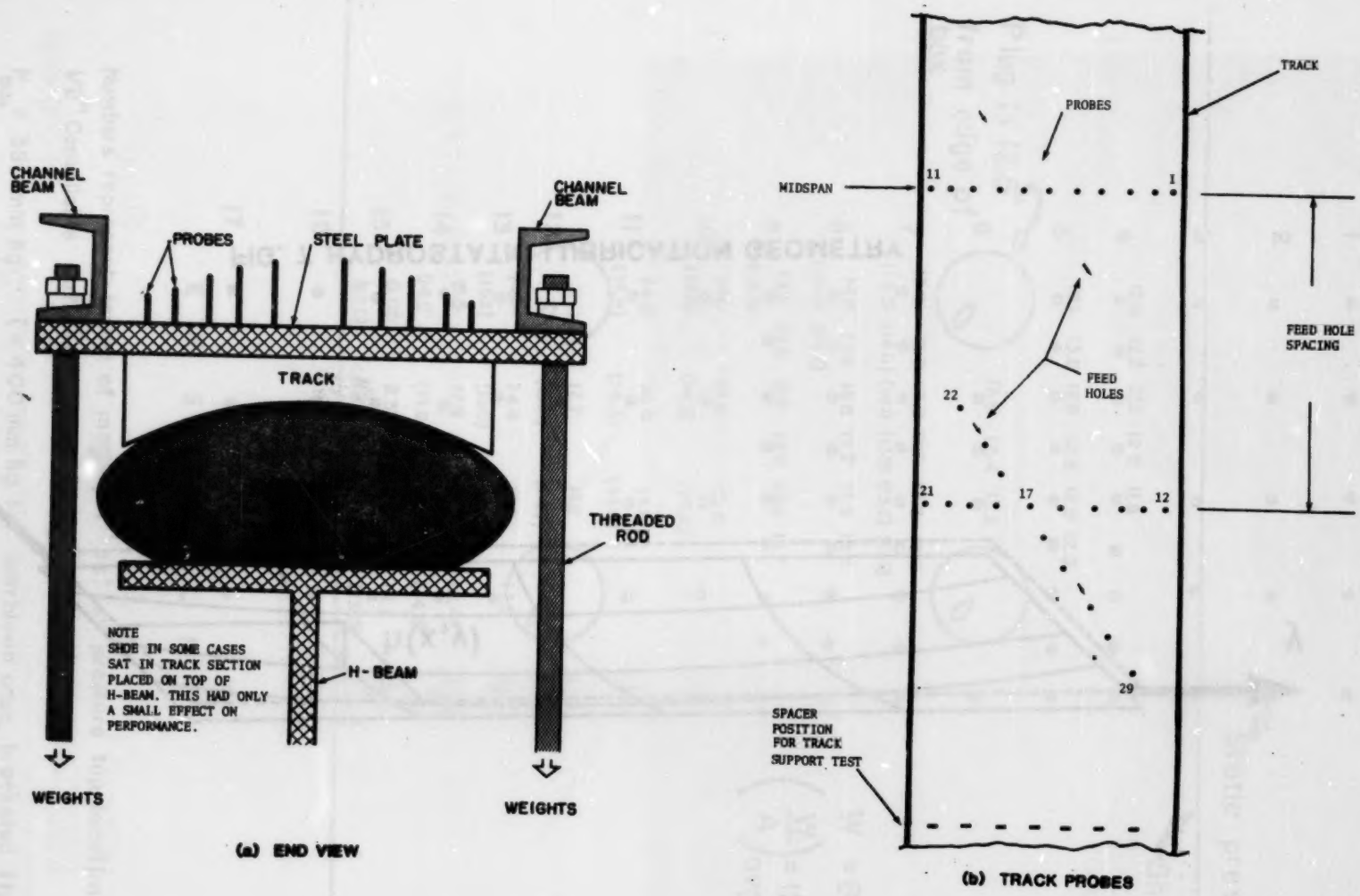

FIG. 8 SCHEMATICS OF GAP MEASUREMENT FACILITY

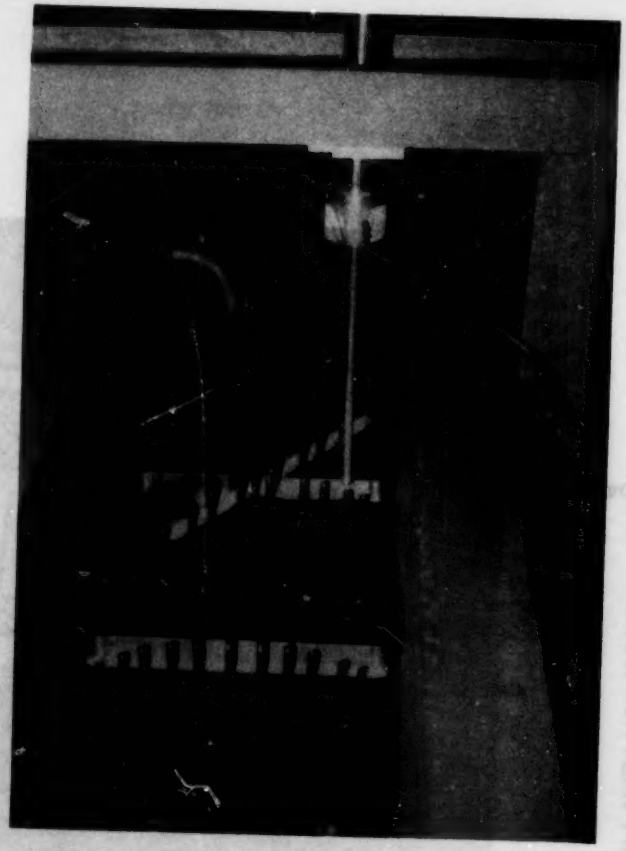

(a) BASIC SETUP

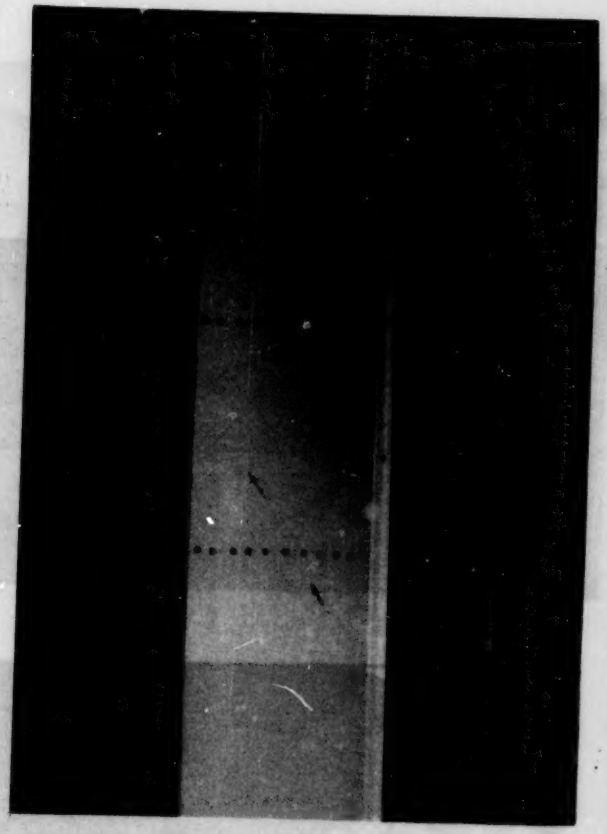

(b) TRACK PROBES

FIG. 9 PICTURES OF GAP MEASUREMENT FACILITY

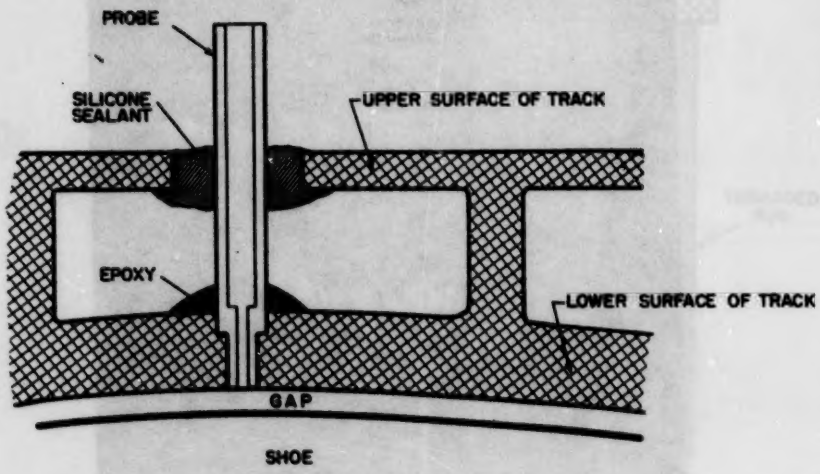

FIG. 10 PROBE CROSS-SECTION

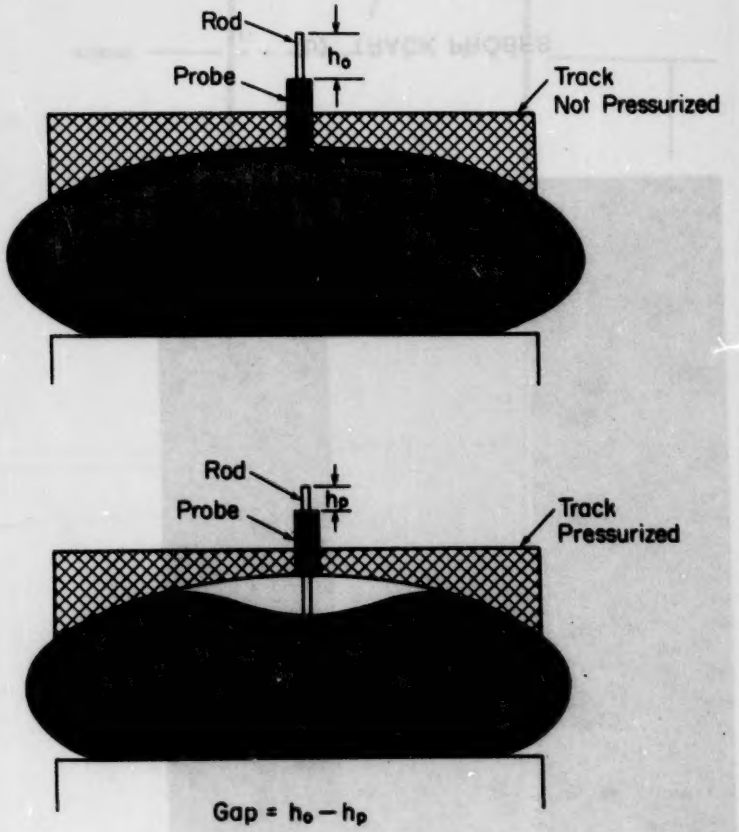

FIG. 11 GAP MEASUREMENT

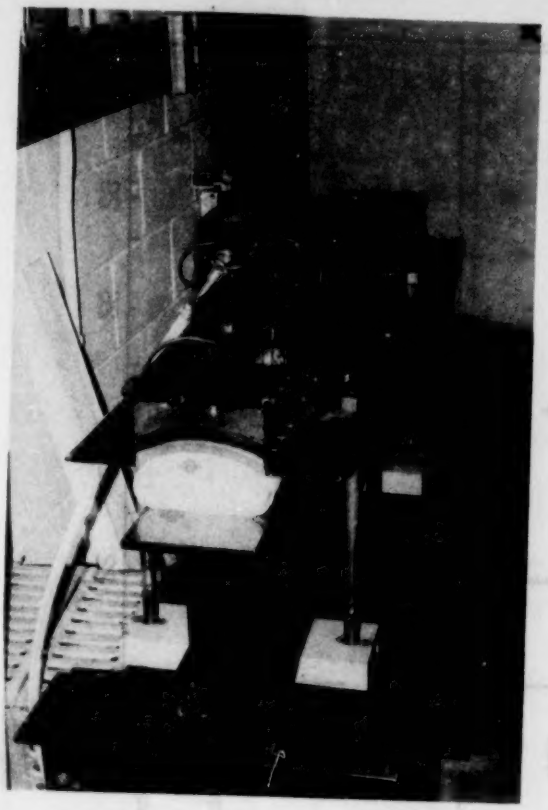

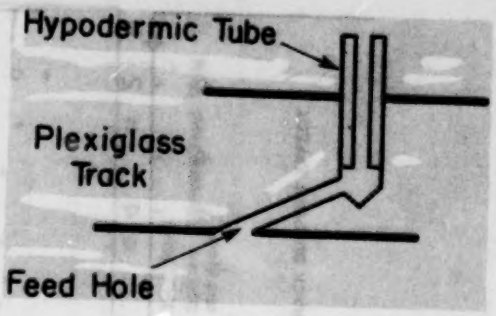

FIG. 12 PICTURE OF FLOW PATTERN FACILITY

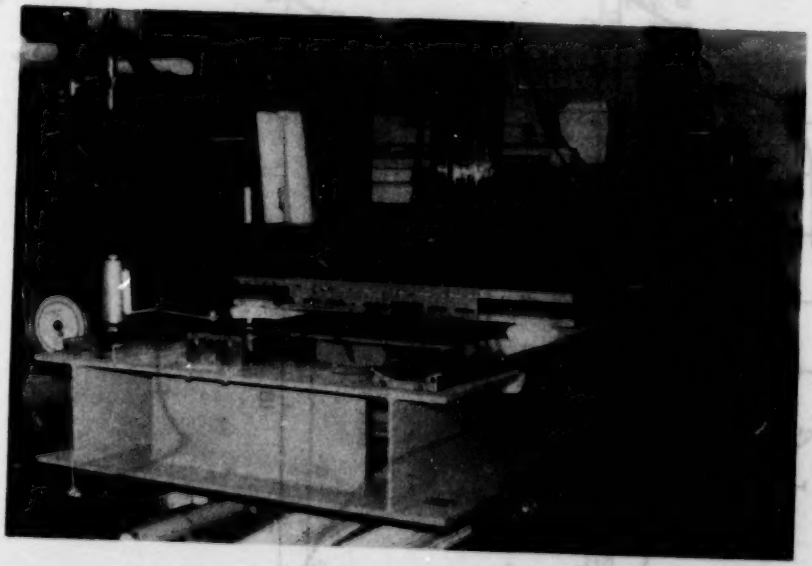

FIG. 13 PICTURE OF PROTOTYPE TEST BED

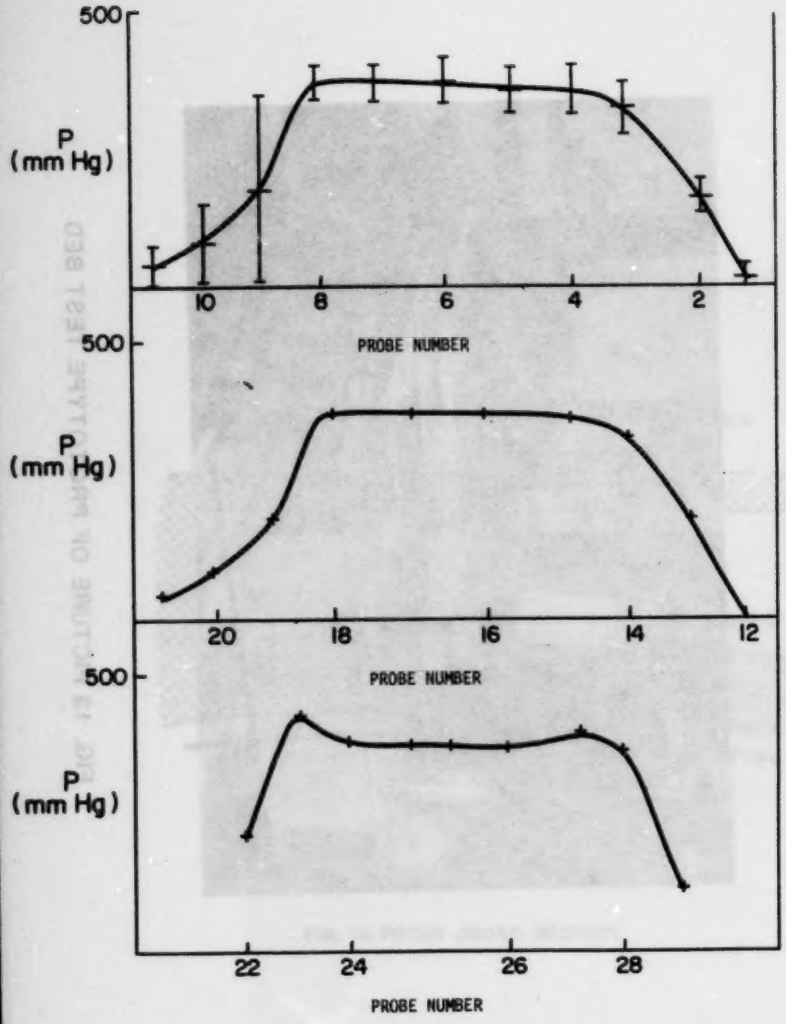

FIG. 14 TYPICAL MEASURED PRESSURE PROFILES

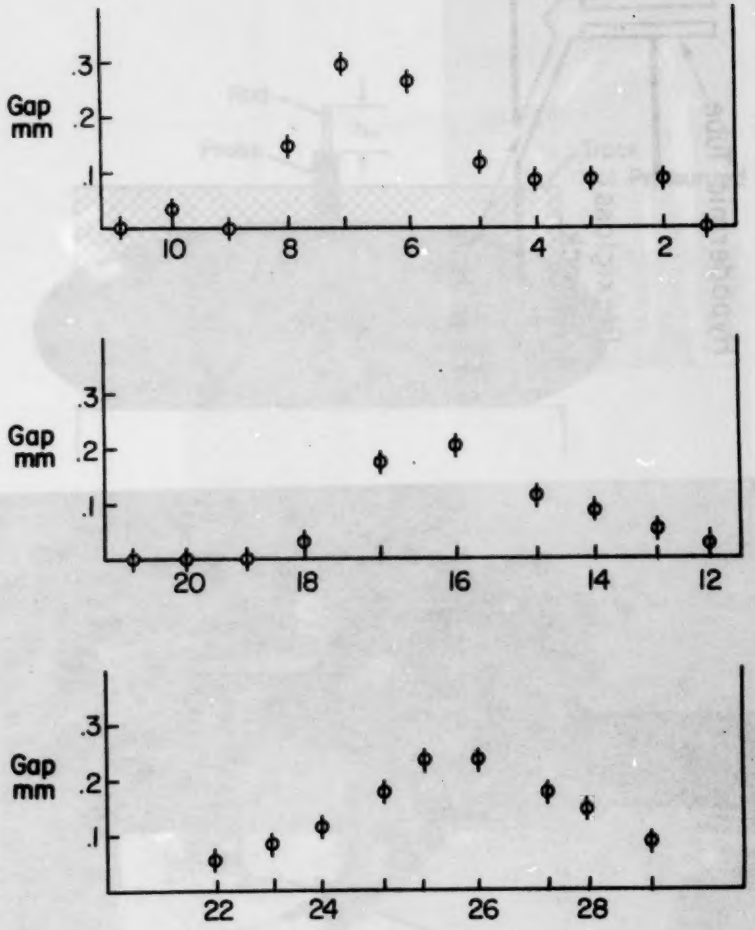

FIG. 15 TYPICAL MEASURED GAP PROFILES

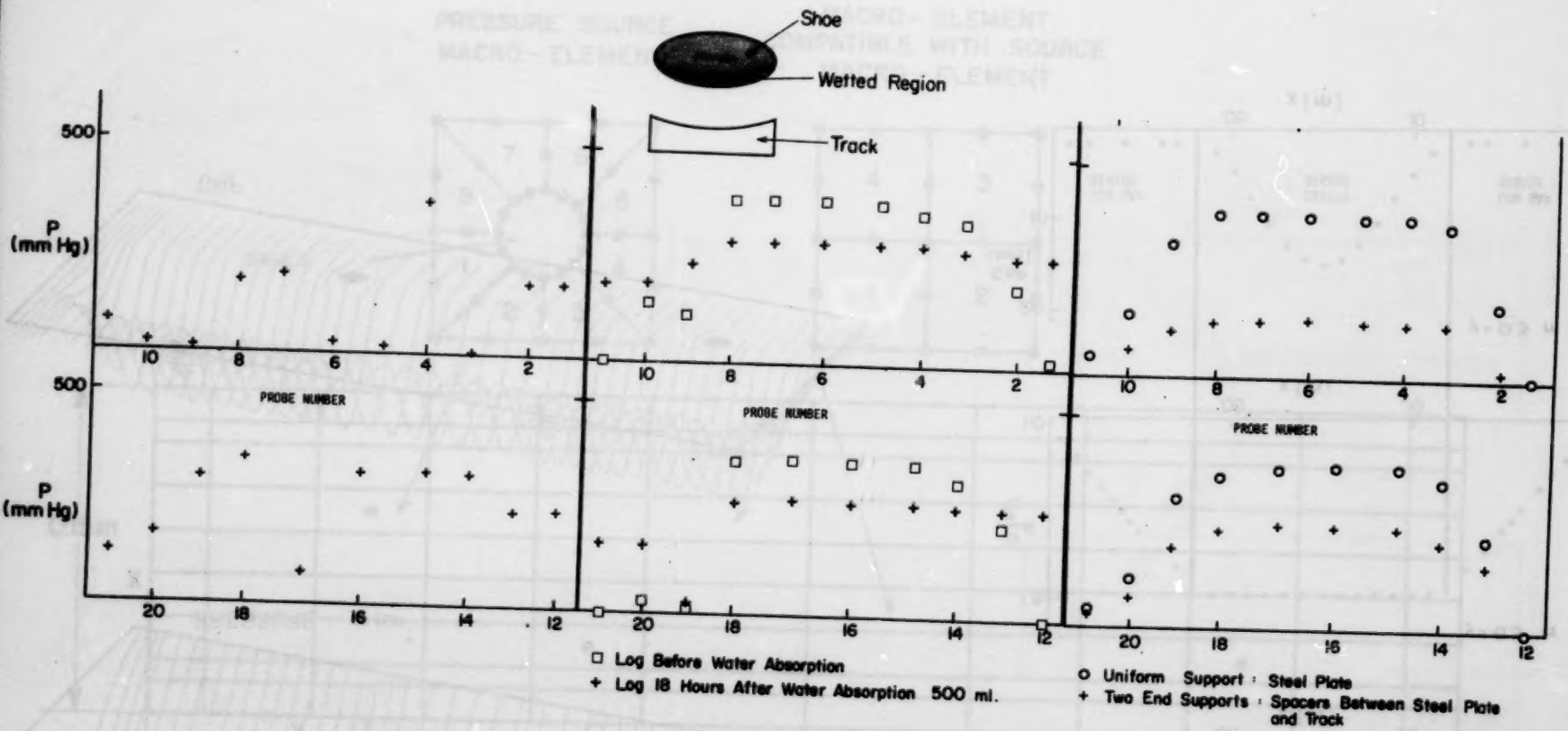

FIG. 16a CARDBOARD TUBE EFFECT

FIG. 16b WATER ABSORPTION EFFECT

FIG. 16c TRACK SUPPORT EFFECT

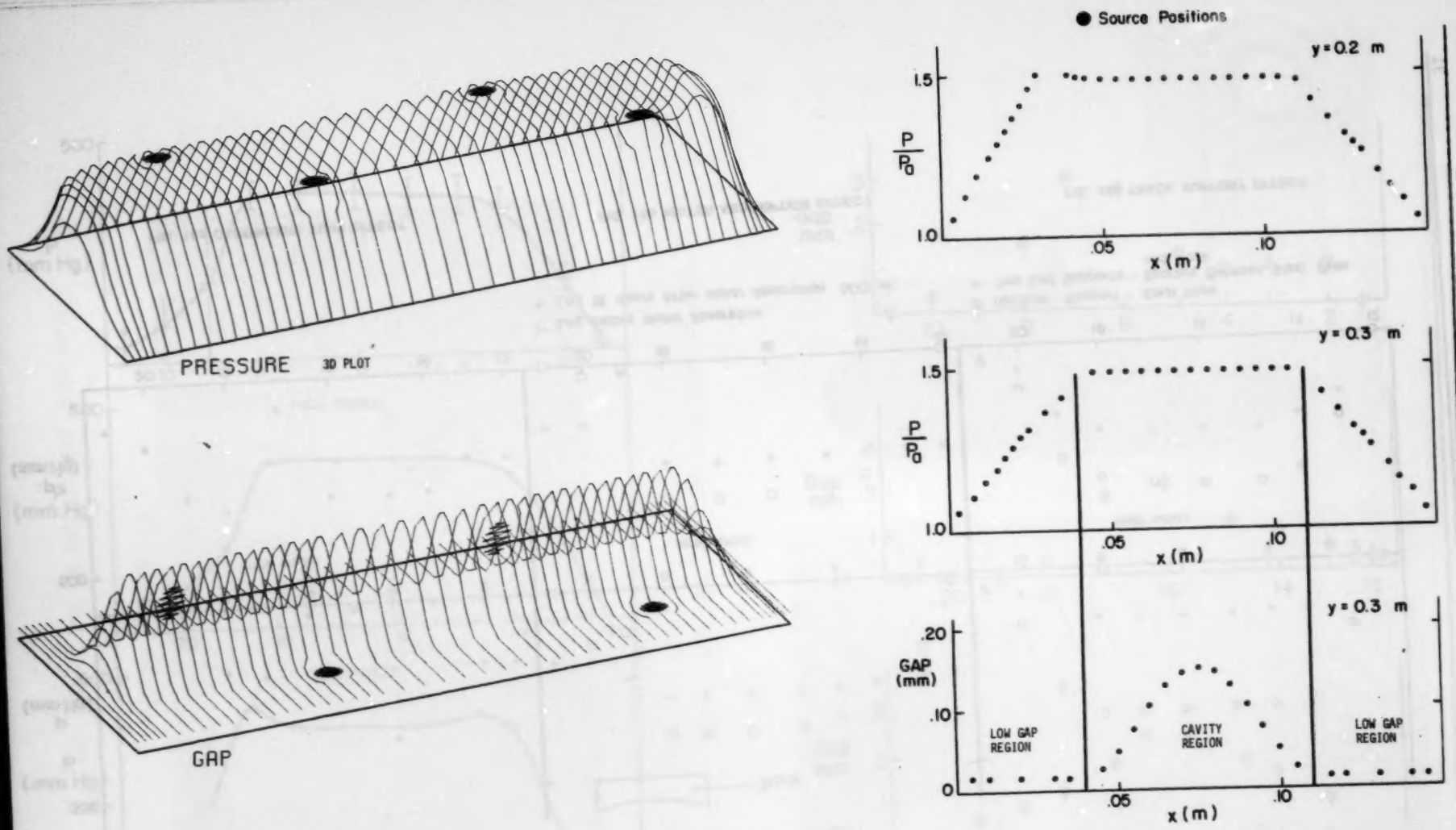

FIG. 17 THEORETICAL PRESSURE DISTRIBUTION FOR ASSUMED GAP DISTRIBUTION QUALITATIVELY SIMILAR TO MEASURED DISTRIBUTION

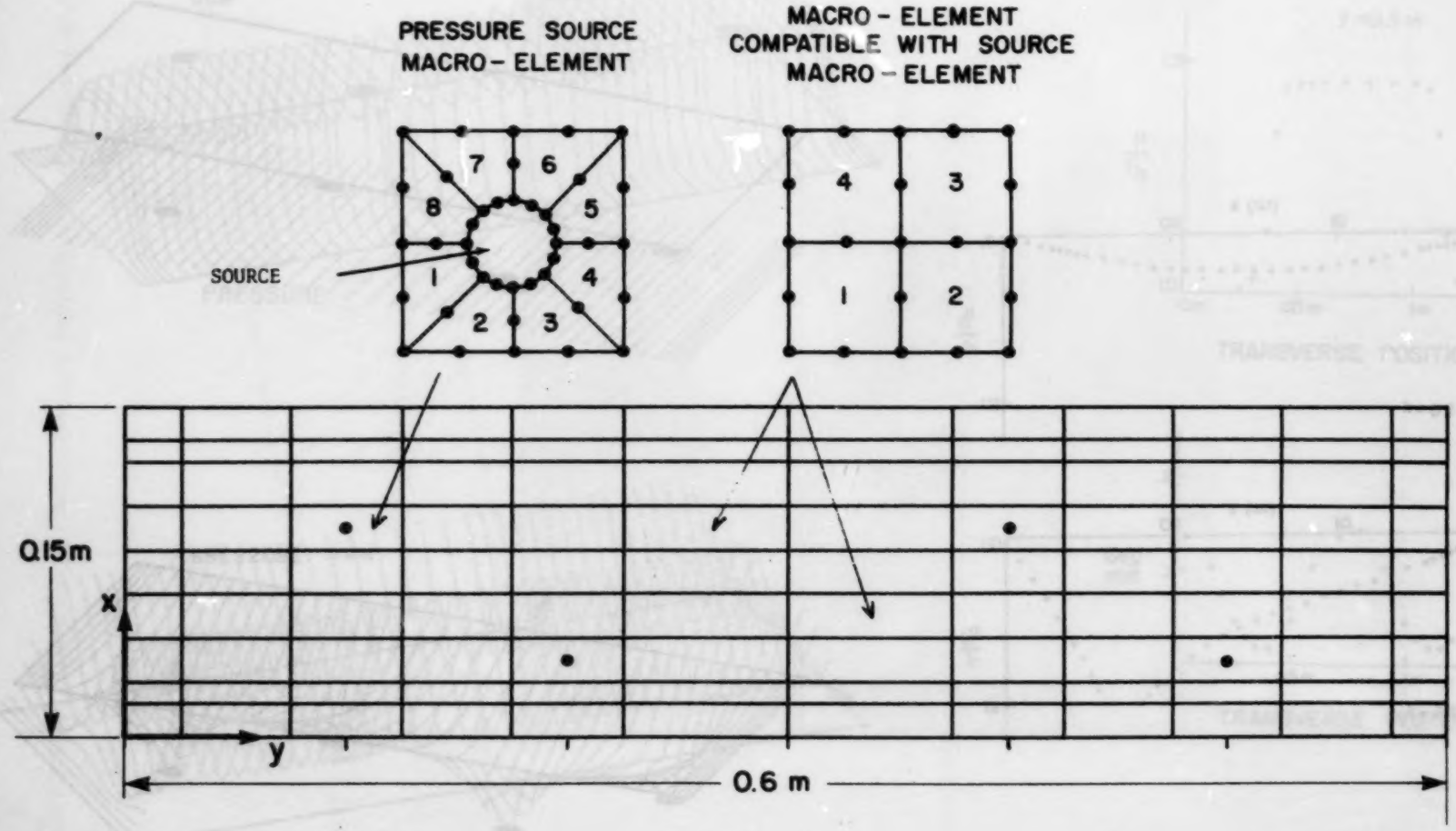

FIG. 18 PRESSURE SOURCE POSITIONS

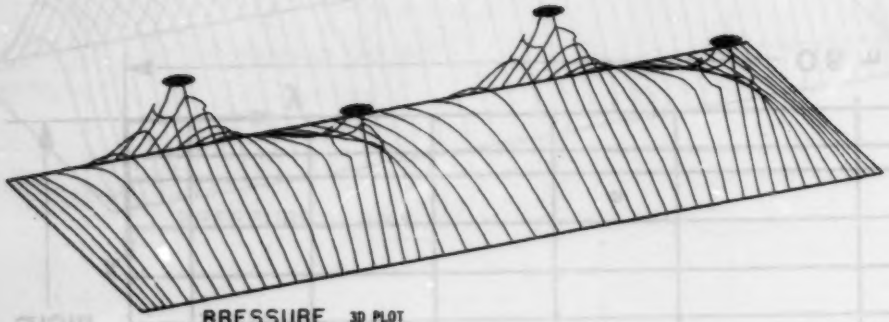

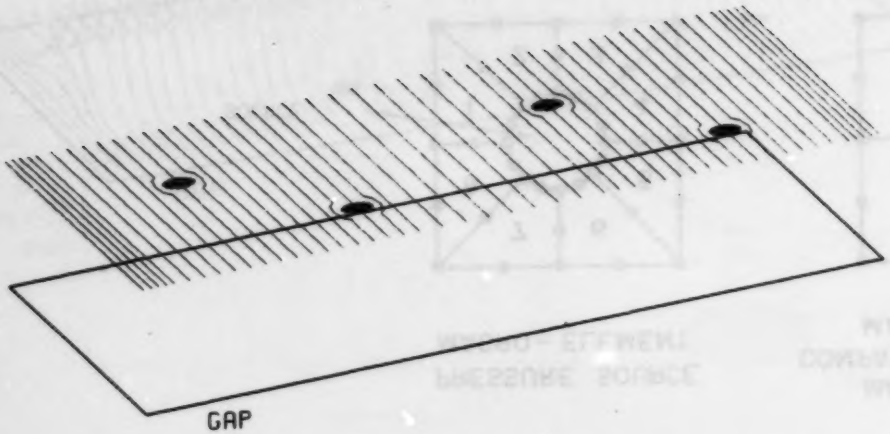

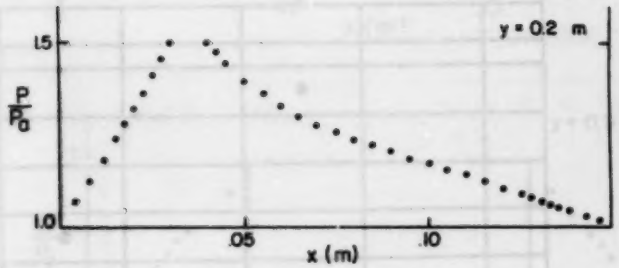

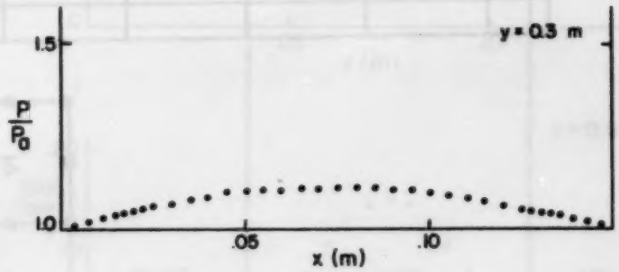

FIG. 19 THEORETICAL PRESSURE DISTRIBUTION FOR UNIFORM GAP DISTRIBUTION

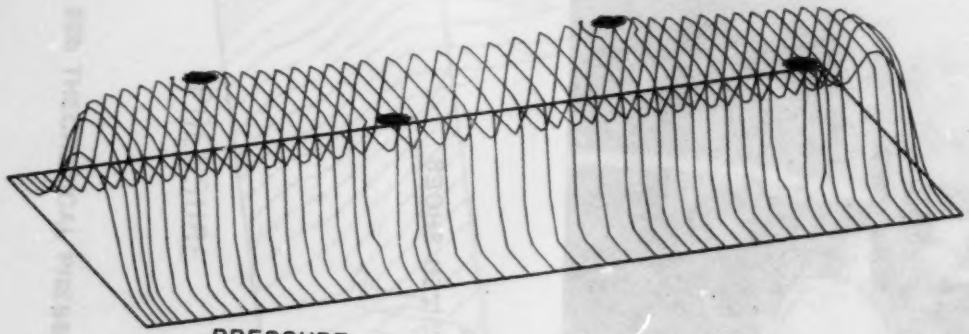

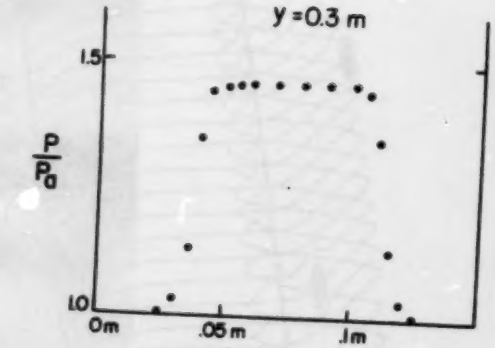

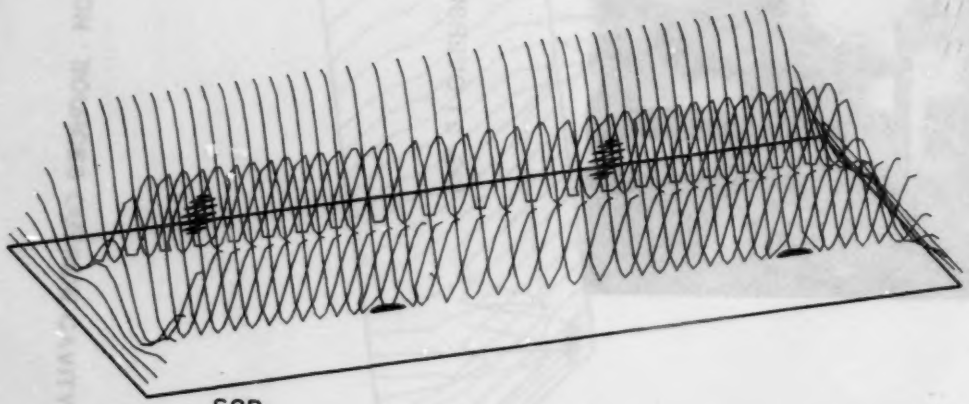

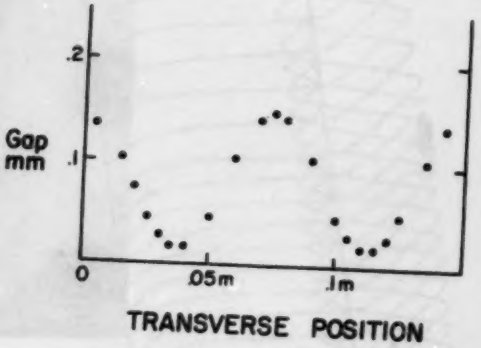

FIG. 20 THEORETICAL PRESSURE DISTRIBUTION FOR OUTER REGION GAP DISTRIBUTION IN WHICH THE GAP INCREASES WITH DISTANCE FROM THE EDGE OF THE CAVITY

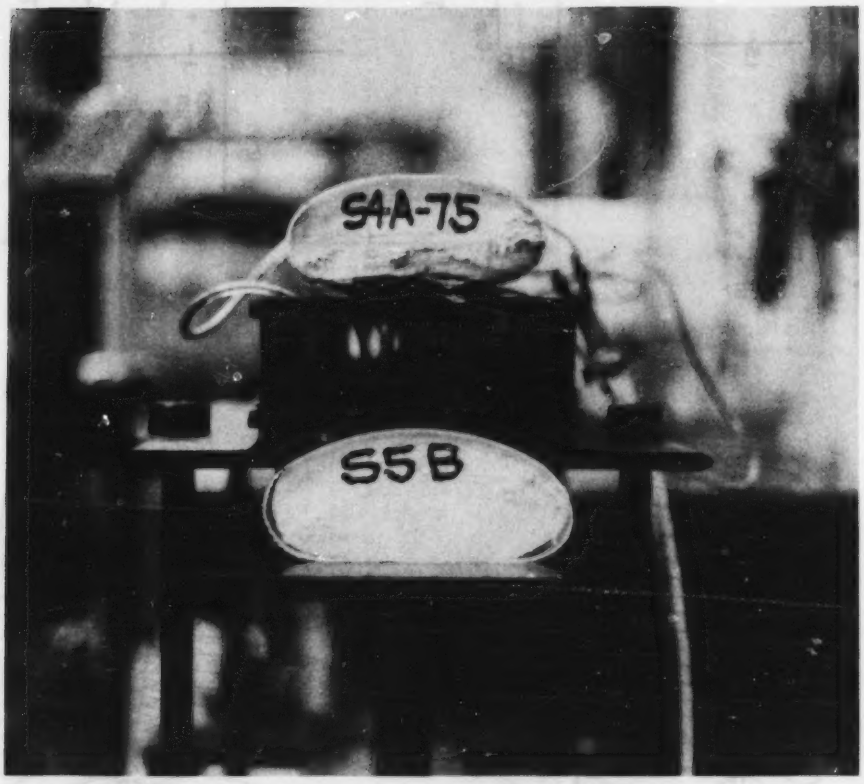

FIG. 21 OVERSIZED AND UNDERSIZED SHOES

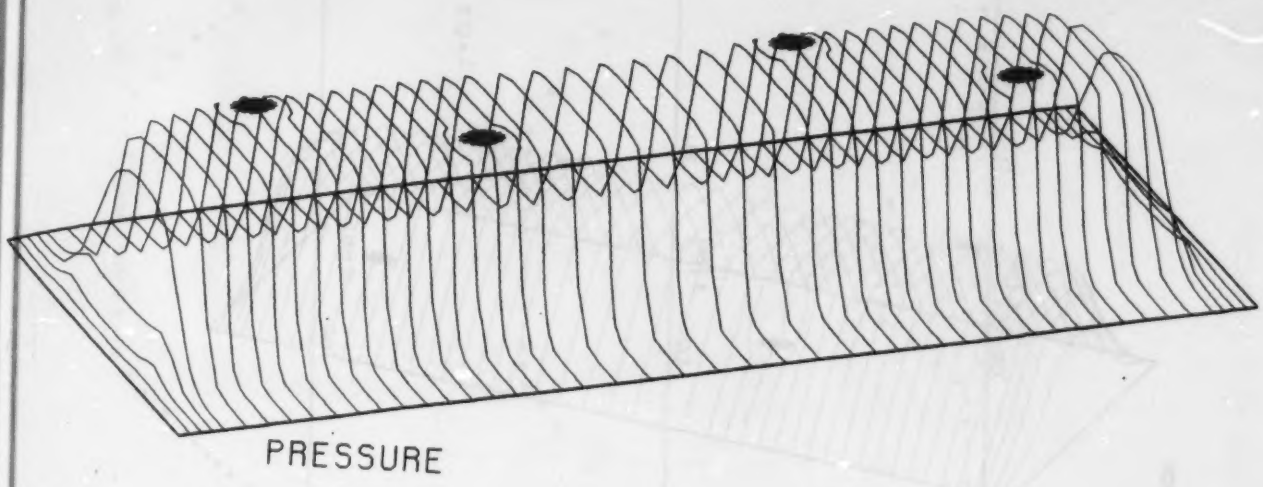

FIG. 22a THEORETICAL PRESSURE DISTRIBUTION : SOURCES WITHIN CAVITY

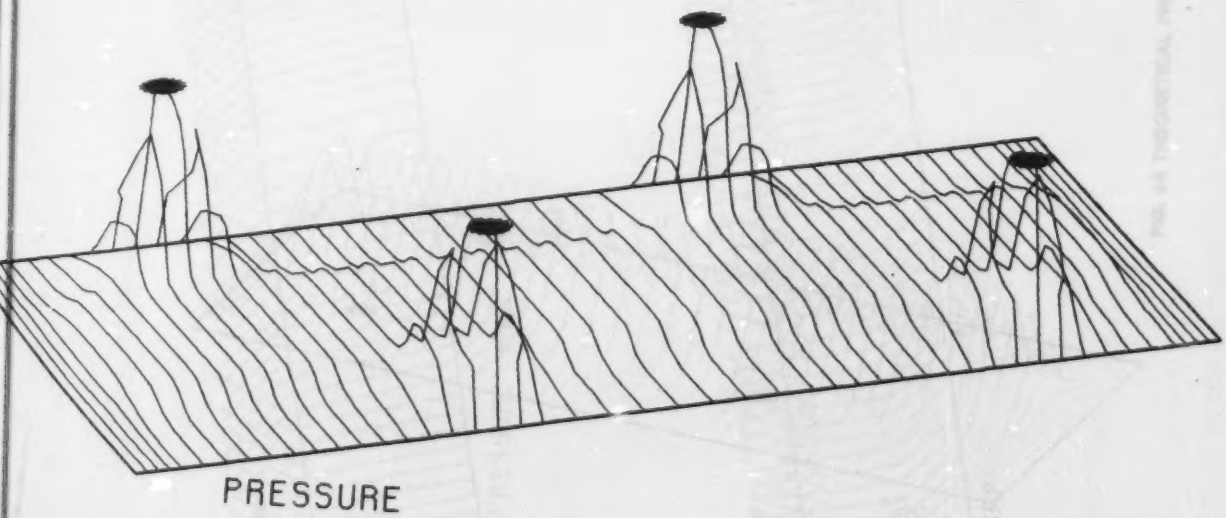

FIG. 22b THEORETICAL PRESSURE DISTRIBUTION : SOURCES OUTSIDE CAVITY

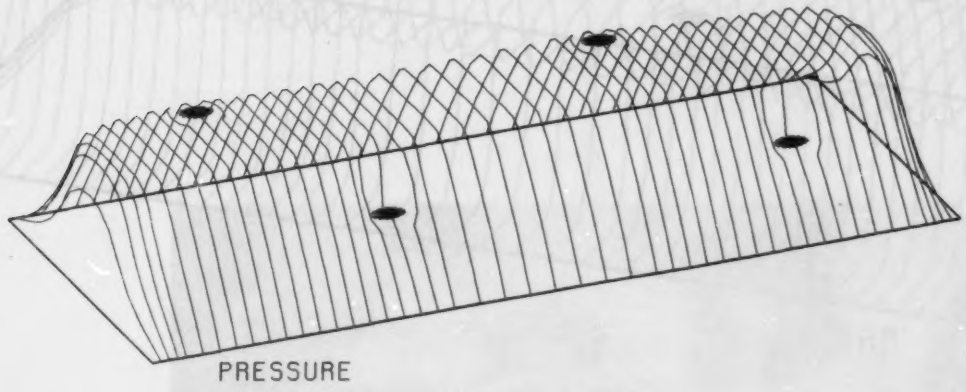

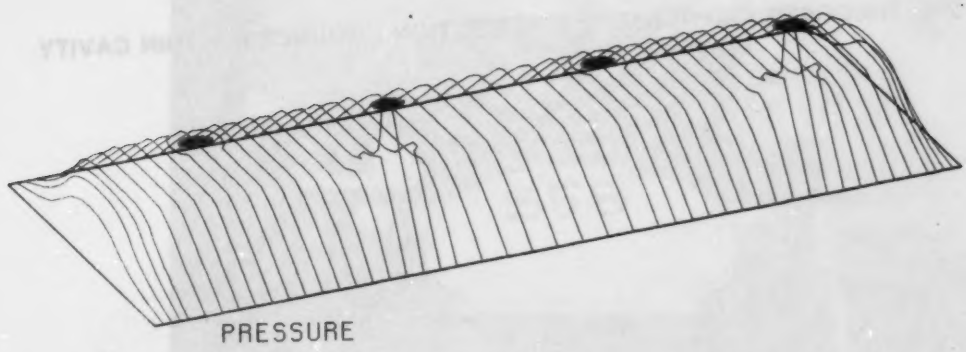

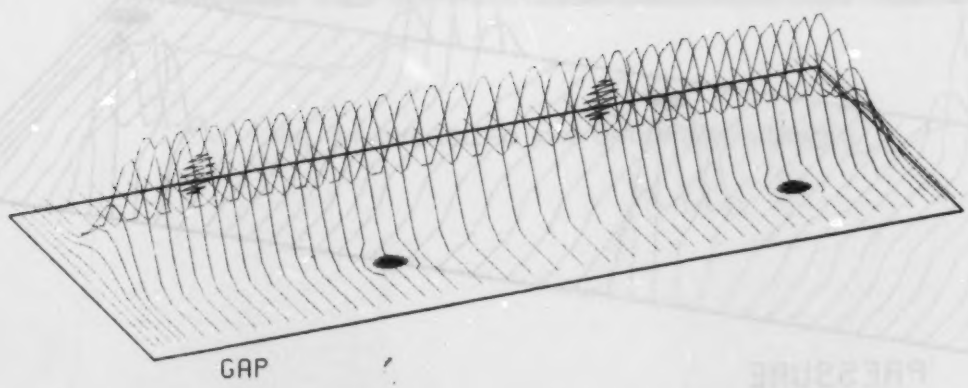

FIG. 23 THEORETICAL PRESSURE DISTRIBUTIONS SHOWING THAT

SOURCES WITHIN CAVITY CONTROL PRESSURE THERE

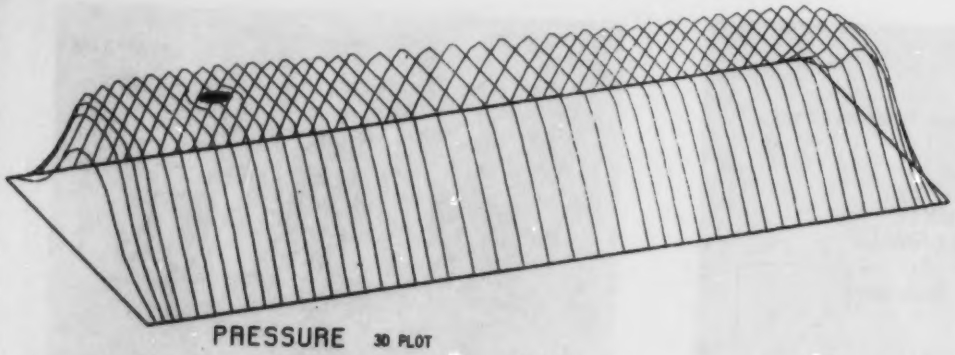

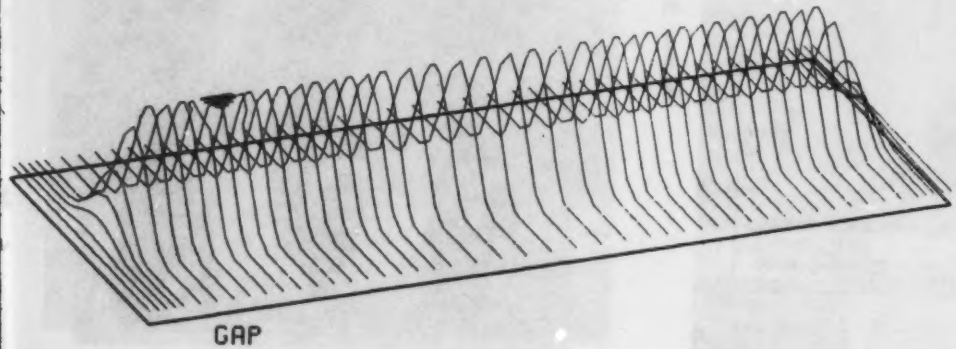

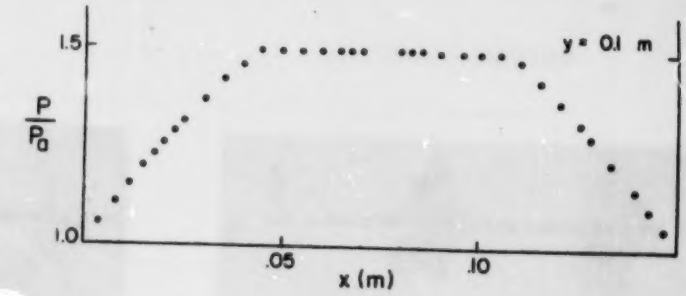

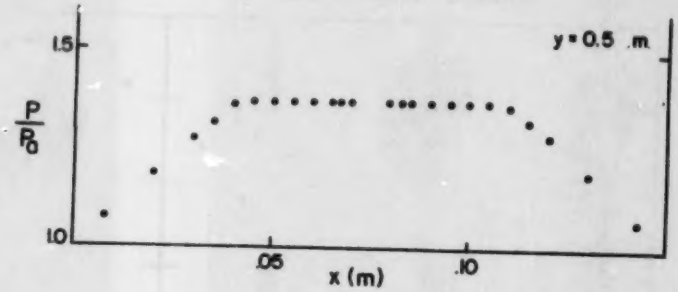

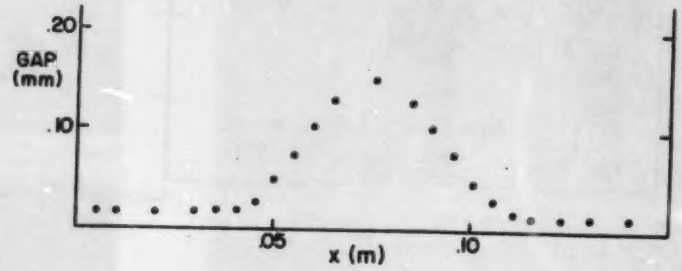

FIG. 24 THEORETICAL PRESSURE DISTRIBUTION FOR ONE PRESSURE SOURCE

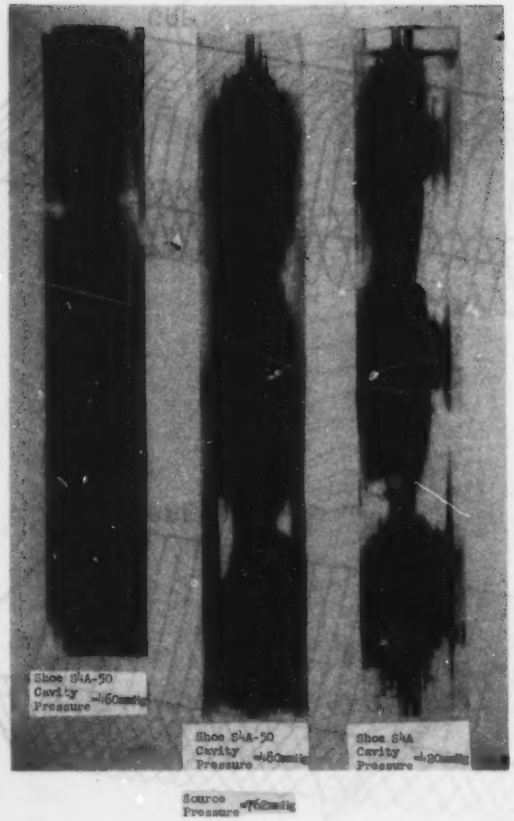

FIG. 25 FLOW PATTERNS OBTAINED ON FLOW PATTERN FACILITY

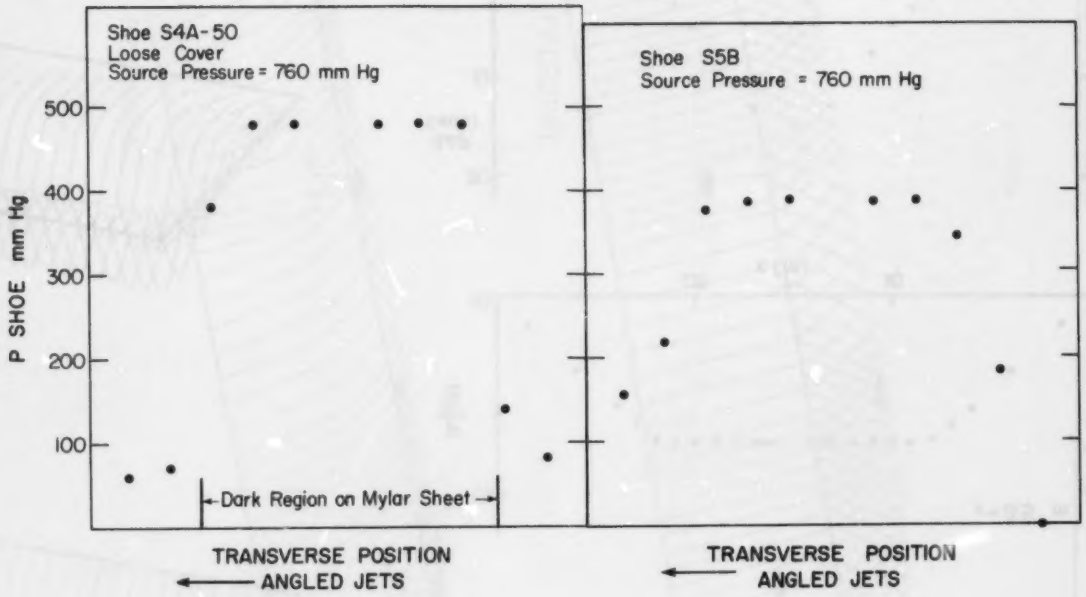

FIG. 26 PRESSURE PROFILE FOR UNDERSIZED SHOE

FIG. 27 PRESSURE PROFILE FOR OVERSIZED SHOE

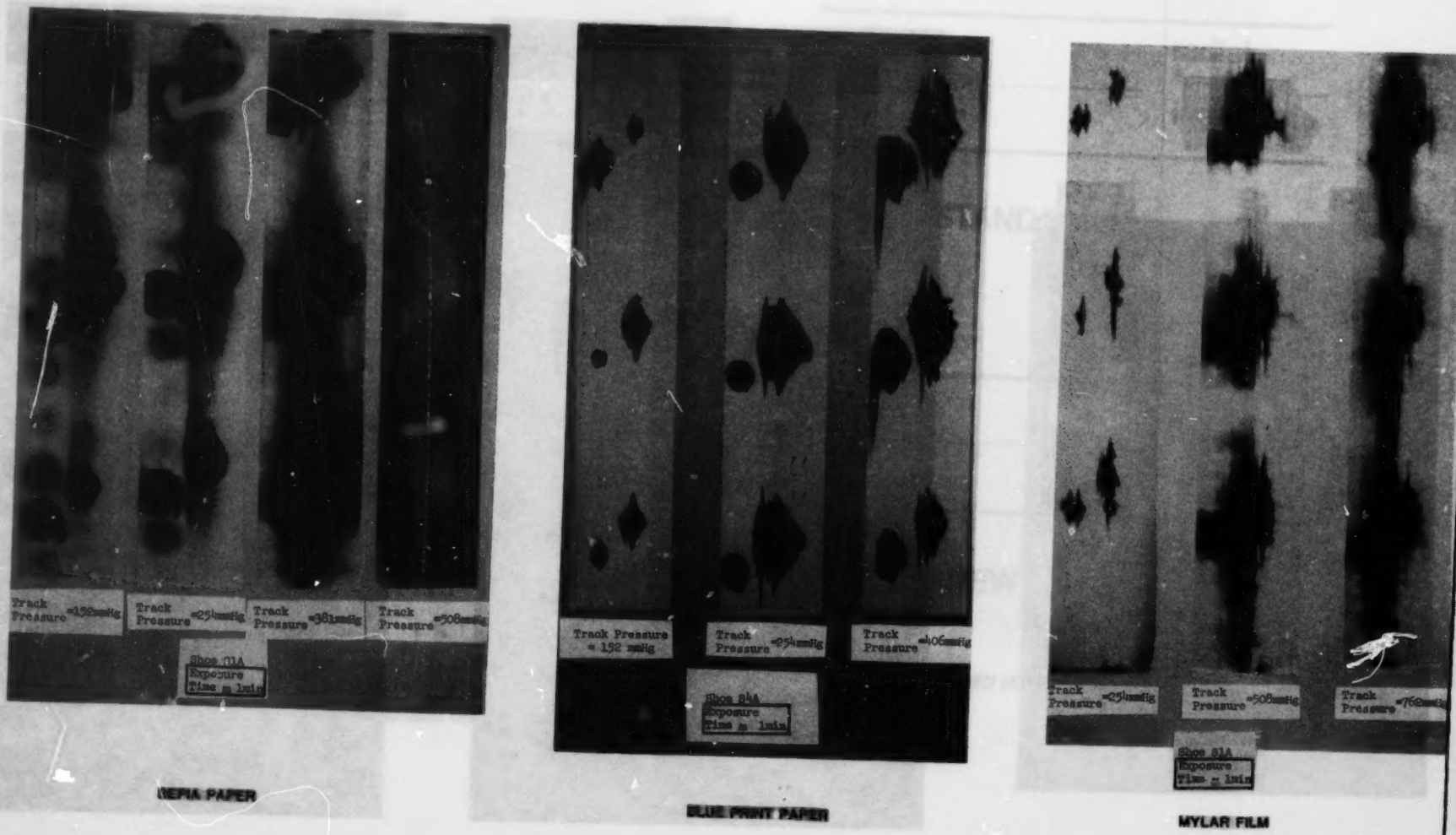

FIG. 28 FLOW PATTERNS OBTAINED FOR ALUMINUM TRACK WITH STANDARD FEED HOLE PATTERN

REPEATABILITY

EXPOSURE TIME COMPARISON

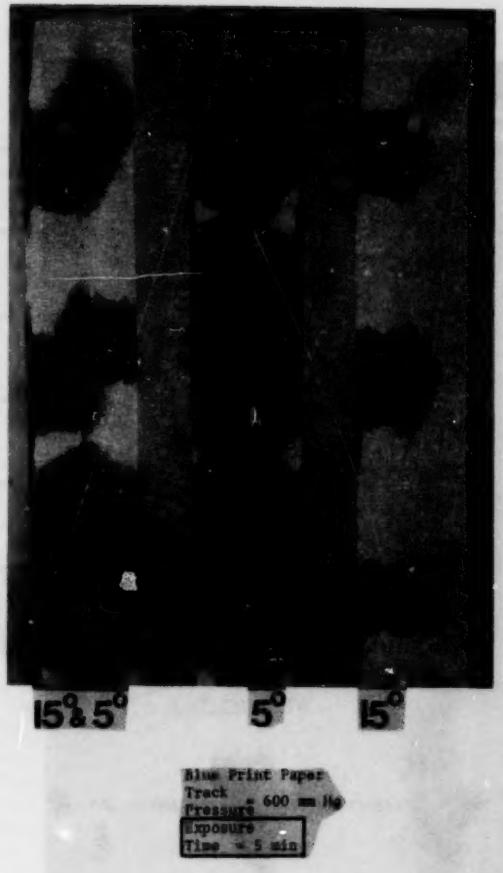

FEED HOLE COMPARISON

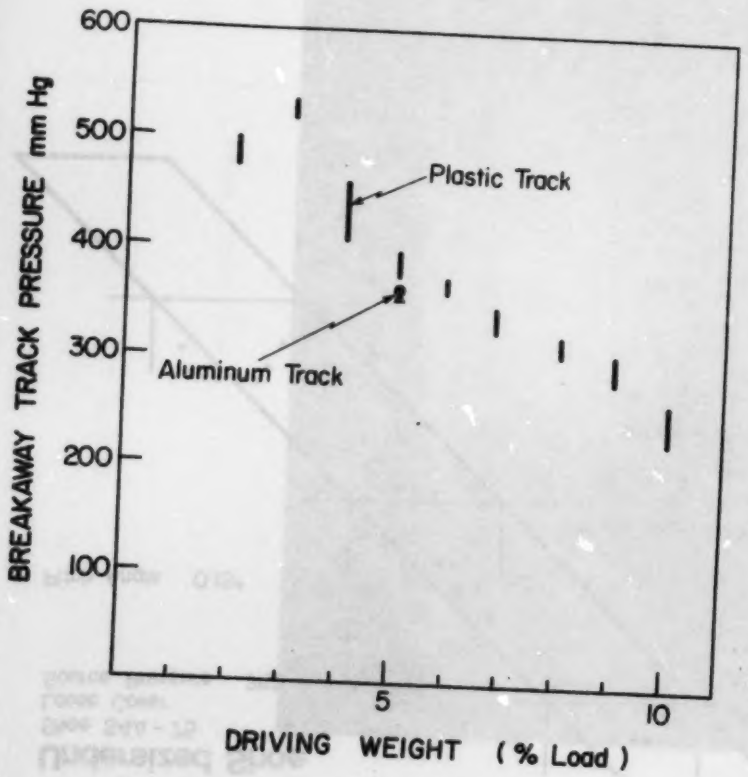

FIG. 29 BREAKAWAY PRESSURE VERSUS DRIVING WEIGHT

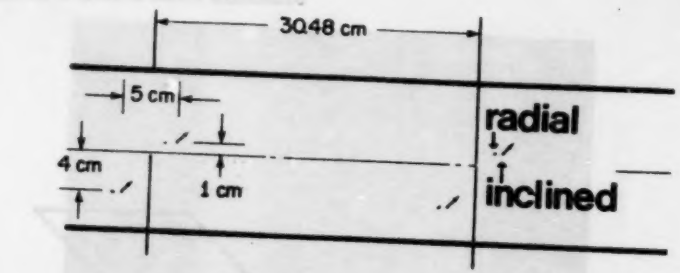

STANDARD

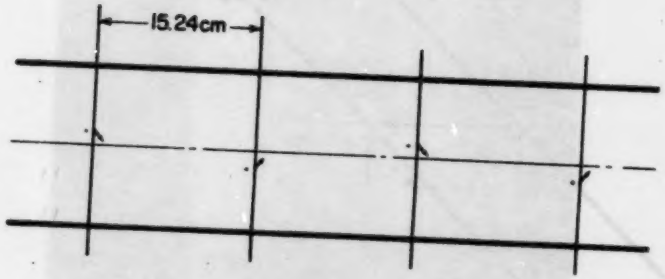

NEW

FIG. 30 FEED HOLE PATTERNS

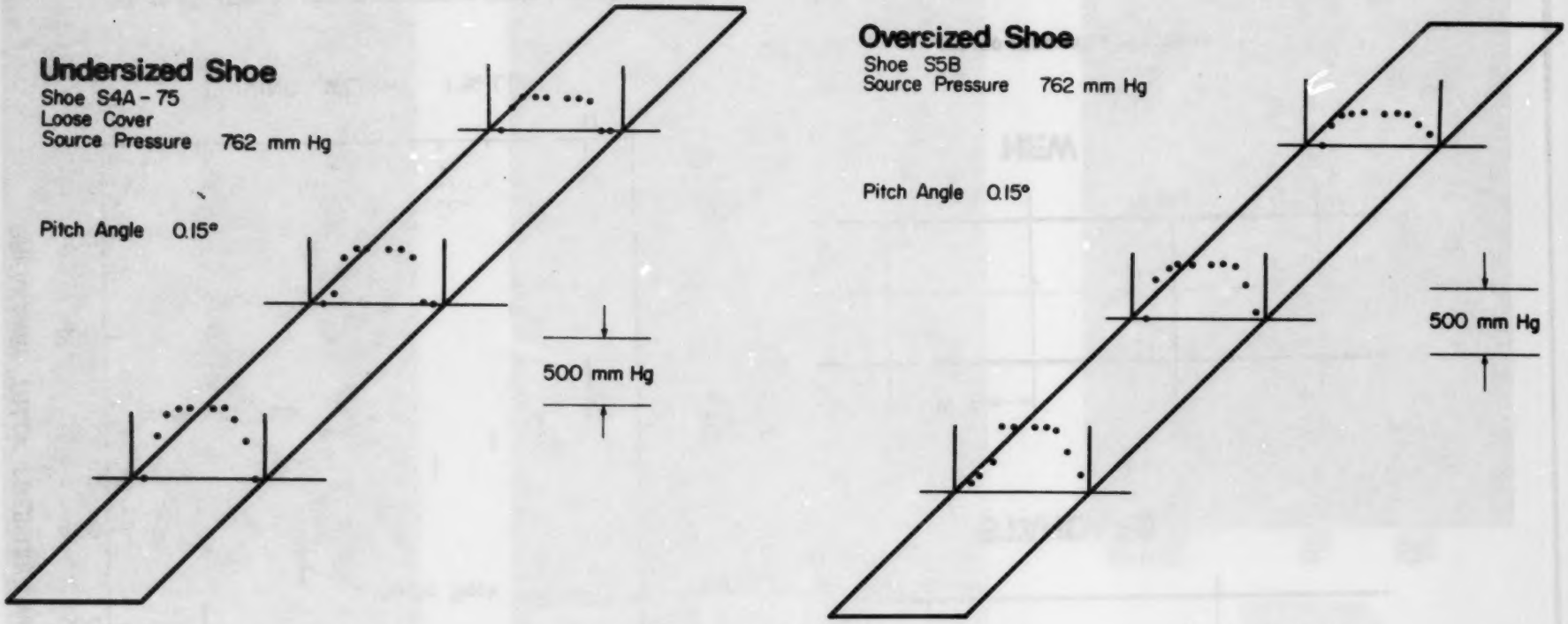

FIG. 31 MEASURED PRESSURE DISTRIBUTIONS SHOWING PITCH STIFFNESS

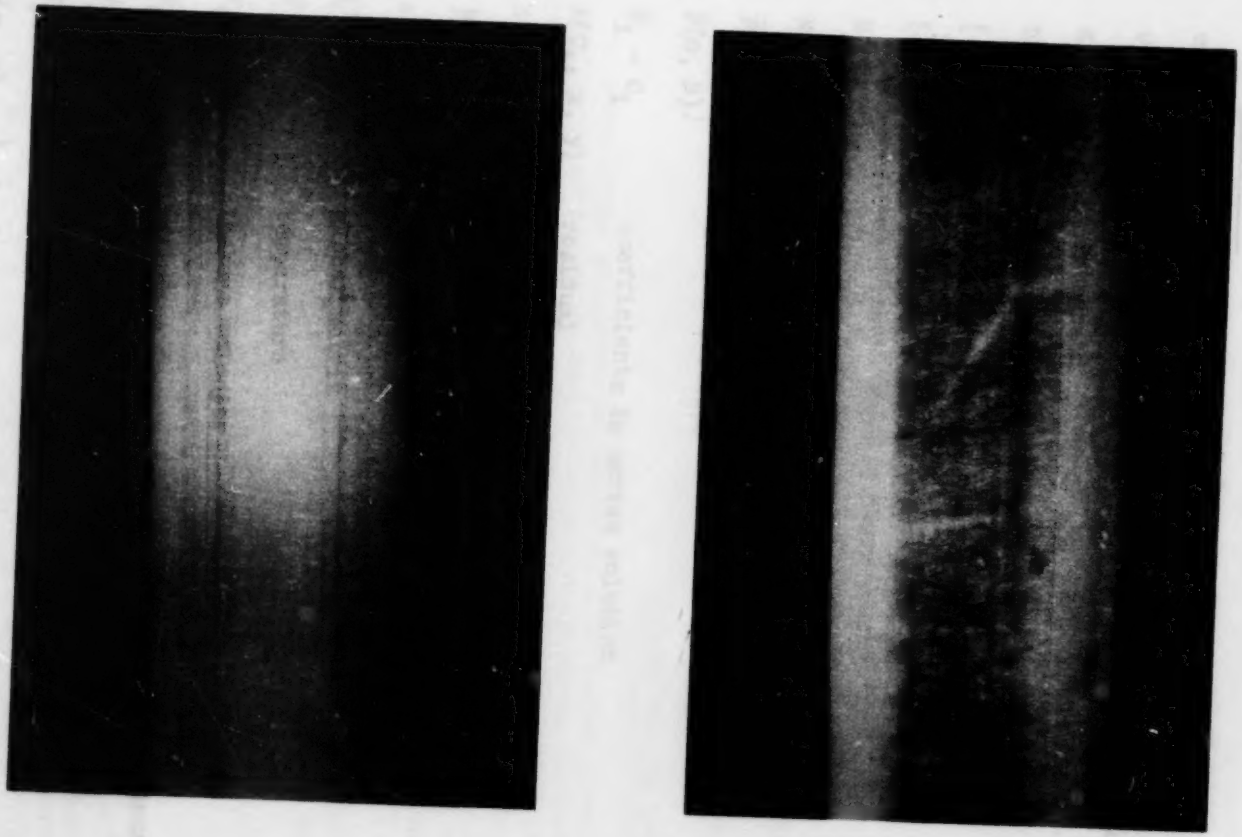

(a) UTIAS

(b) E.B.EDDY

FIG. 32 SCRATCH MARKS ON SHOES

Notation

c	contour integral
C_i	coefficients in finite element series solution
$g_j(C_i, \alpha, \beta)$	integrand
$h(x, y)$	gap between shoe and track
$[J]$	Jacobian matrix
$[K]_k$	element contribution
$N_i(x, y)$, $N_i(\alpha, \beta)$	shape functions in series solution
$\tilde{P}(x, y)$, $\tilde{P}(\alpha, \beta)$	series solution
$\tilde{P}_i = C_i$	coefficients in series solution
$R(C_i, x, y)$	residual
R	gas constant
$\|R\|$	load vector
s	surface integral
$[S]$	global matrix
T	temperature
v_d	leakage velocity
W_f	weighting factor for line integration by Gaussian Quadrature
$W_j(x, y)$, $W_j(\alpha, \beta)$	weighting functions
$\bar{u}(x, y)$, $\bar{v}(x, y)$	mean velocities
x, y	global coordinate system

α, β	local coordinate system
μ	laminar viscosity
ρ	air density

Subscripts

i	node
j	weighting function
k	element

A.1 THE FINITE ELEMENT METHOD

The finite element method is a technique for obtaining approximate solutions to differential equations for which analytical solutions are either not possible or very tedious to obtain. This could be due to irregular system geometries, nonlinearities in the governing differential equations, or a combination thereof. The SailRail problem falls into the third class. As presented here, the technique is just an application of Galerkin's method, which is in turn just one of a number of approximate methods contained within the methods of weighted residuals [A1].

For the SailRail problem, one seeks by the Galerkin technique an approximate solution for pressure of the form (see Figure A1)

$$\tilde{P}(x, y) = \sum_{i=1}^{n} C_i N_i(x, y) \qquad \text{(A1.1)}$$

where the functions $N_i(x, y)$ are members of a complete set of specified functions [A1]. The adjustable constants C_i must be chosen so that the governing differential equation is satisfied in some average sense over the entire solution domain. For this, the assumed solution is substituted into the governing differential equation to obtain the generally nonzero residual $R(C_i, x, y)$. By choosing weighting functions $W_j(x, y) = N_j(x, y)$ and writing

$$\int_S W_j(x, y) R(C_i, x, y) dxdy = 0 \qquad j = 1, \ldots, n \qquad \text{(A1.2)}$$

this residual is made orthogonal to members of the complete set of basis functions to which the functions $N_i(x, y)$ belong. The completeness property

is necessary for convergence to the true solution because only linear combinations of members of a complete set of functions have the inherent capability of filling the space of all possible solutions as their number tends to infinity. One can think of the Galerkin procedure as a projection operator which projects the exact solution from an infinite dimensional space into a finite dimensional subspace. Note that any square integrable function is zero if it is orthogonal to every member of a complete set of functions [A1]. It is this fact which is exploited in equation (A1.2). When evaluated, the weighted integral expressions give a system of algebraic equations for the constants C_i.

One distinguishing feature of a finite element Galerkin analysis is its shape functions $N_i(x, y)$ are not infinitely differentiable. In particular, there are discontinuities in certain derivatives of $N_i(x, y)$ at element interfaces. Another distinguishing feature of a finite element analysis is for computational purposes each global weighted integral expression is subdivided into a sum of element or local contributions as follows:

$$\underbrace{\int_S W_j(x,y)R(C_i,x,y)dxdy}_{\substack{\text{Global}\\ \text{Weighted}\\ \text{Integral}\\ \text{Expression}}} = \sum_{k=1}^{m} \underbrace{\int_{S_k} W_{jk}(x,y)R(C_i,x,y)dxdy}_{\substack{\text{Local}\\ \text{Contribution}}} \qquad \text{(A1.3)}$$

where the subscript "k" refers to a particular element k and "m" is the number of elements. Each element is considered in turn and its contributions to various global expressions are calculated and assembled into the global algebraic equation system.

A.2 GOVERNING EQUATION FOR AIR FLOW

The geometry under consideration is shown schematically in Figure A1. The assumptions used for the derivation of the differential equation governing the generation of air pressure in the gap between the shoe and track are as follows [A2]:

a) Compared to viscous and pressure effects, inertia effects are negligible. This assumption would probably not be valid at a feed hole.

b) Curvature of the surfaces introduces only second-order effects.

c) The air film is so thin that the derivatives of velocity across the film thickness are far more important than any of the other velocity derivatives. This is the so-called thin-film approximation.

d) Variable viscosity need not be considered because air bearings have very low shear losses and the viscosity of air is relatively unaffected by the slight spatial temperature variations which may exist.

e) The bearing operates in the isothermal state at some characteristic operating temperature.

With these assumptions, the conservation equations of mass and momentum can be manipulated to obtain the Reynolds equation [A2]

$$\nabla \cdot \left\{ \frac{\rho h^3}{12\mu} \nabla P \right\} =$$

$$\nabla \cdot (\rho h U) + \frac{\partial}{\partial t} (\rho h) + \rho v_d \qquad \text{(A2.1)}$$

forward motion effect	heave motion effect	leakage flow effect

For the present work, the effects of forward motion, heave motion and leakage flow are assumed absent. With these assumptions and the ideal gas law, $P = \rho RT$, the Reynolds equation reduces to

$$\nabla \cdot (Ph^3 \nabla P) = 0 \qquad \text{(A2.2)}$$

Note that the above equation is nonlinear. This complicates the solution algorithm. Note also that if the gap "h" is uniform throughout, equation (A2.2) further reduces to

$$\nabla \cdot (P \nabla P) = 0 \qquad \text{(A2.3)}$$

In other words, the pressure distribution would in this case be independent of the magnitude of "h". Furthermore, equation (A2.2) shows that scaling the gap distribution by some constant factor would not affect the pressure distribution.

Equation (A2.2) follows directly from the continuity equation

$$\frac{\partial}{\partial x} (\rho h \bar{u}) + \frac{\partial}{\partial y} (\rho h \bar{v}) = 0 \qquad \text{(A2.4)}$$

when the momentum equations for purely viscous planar flow are used to obtain the mean velocities $\bar{u}$ and $\bar{v}$

$$\bar{u} = -\frac{\partial p}{\partial x}\frac{h^2}{12\mu} \tag{A2.5}$$

$$\bar{v} = -\frac{\partial p}{\partial y}\frac{h^2}{12\mu} \tag{A2.6}$$

Substitution of these expressions and the ideal gas law for isothermal flow into (A2.4) gives

$$\frac{\partial}{\partial x}\left(Ph^3\frac{\partial p}{\partial x}\right) + \frac{\partial}{\partial y}\left(Ph^3\frac{\partial p}{\partial y}\right) = 0 \tag{A2.7}$$

which is Reynolds' equation.

A.3 APPLICATION OF GALERKIN'S METHOD

A.3.1 Elements

Quadratic isoparametric rectangular elements were chosen for the present work [A2]. In the global coordinate system defined by x and y, a typical element is as shown in Figure A2. When transformed into a local coordinate system using the isoparametric transformation, it is as shown in Figure A3. In the local coordinate system pressure is assumed to vary quadratically according to

$$\tilde{P}(\alpha, \beta) = \sum_{i=1}^{8} N_i(\alpha, \beta)C_i \tag{A3.1}$$

where the local node shape functions $N_i(\alpha, \beta)$ are given by

$$N_i(\alpha, \beta) = \frac{1}{4}(1 + \alpha\alpha_i)(1 + \beta\beta_i)(\alpha\alpha_i + \beta\beta_i - 1)$$

where

$$\alpha_i = \pm 1,\ \beta_i = \pm 1$$

$$N_i(\alpha, \beta) = \frac{1}{2}(1 - \alpha^2)(1 + \beta\beta_i) \tag{A3.2}$$

where

$$\alpha_1 = 0, \quad \beta_i = \pm 1$$

$$N_i(\alpha, \beta) = \frac{1}{2}(1 + \alpha\alpha_i)(1 - \beta^2)$$

where

$$\alpha_i = \pm 1, \quad \beta_i = 0$$

The subscript "i" refers to a particular local node i. Note that each local function $N_i(\alpha, \beta)$ is unity at node i but zero at the other nodes (see Figure A4). This means that at node i, $\tilde{P}_i = C_i$. Thus, a coefficient in the finite element expansion has a direct physical significance and is the pressure at a particular node. The isoparametric transformation from the local coordinate system to the global coordinate system is based on [A2].

$$x = \sum_{i=1}^{8} N_i(\alpha, \beta)x_i$$

$$y = \sum_{i=1}^{8} N_i(\alpha, \beta)y_i \qquad \text{(A3.3)}$$

where again the subscript "i" refers to local node i. In other words, the shape functions used for representing pressure within an element are also used to represent the element shape in the global coordinate system.

When the assumed element variation of $\tilde{P}(x, y)$ is substituted into the Reynolds equation for pressure and the resulting residual is weighted by the weighting function $W_j(x, y) = N_j(x, y)$ and then integrated over the element, one obtains the local contribution

$$\int_S W_j \left[\nabla \cdot \left\{ \tilde{P}h^3 \nabla \tilde{P} \right\} \right] dxdy \qquad \text{(A3.4)}$$

Here, this is manipulated to obtain

$$-\int_S \left[\nabla W_j \cdot \tilde{Ph}^3 \nabla \tilde{P} \right] dxdy + \int_c W_j \, \tilde{Ph}^3 \frac{\partial \tilde{P}}{\partial n} \, dc \qquad (A3.5)$$

The reason for this manipulation is functional analysis shows that it would otherwise be necessary to have both pressure and its first derivatives continuous across the element interfaces [A2]. The integration by parts allows one to shift some of the continuity requirements onto the weighting functions W_j. Then, only pressure need be continuous across the element interfaces. For the SailRail problem, the boundary conditions are such that the contour integral can be ignored at any boundary. It can also be ignored at element interfaces because the contribution to it from one element cancels the contribution from a neighbouring element [A2]. Thus, a typical local weighted integral expression reduces to

$$\int_S \left[\nabla W_j \cdot \tilde{Ph}^3 \nabla \tilde{P} \right] dx \, dy \qquad (A3.6)$$

Now

$$\frac{\partial \tilde{P}}{\partial x} = \sum_{i=1}^{8} \frac{\partial N_i}{\partial x} P_i$$

$$\frac{\partial \tilde{P}}{\partial y} = \sum_{i=1}^{8} \frac{\partial N_i}{\partial y} P_i \qquad (A3.7)$$

One can obtain $\frac{\partial N_i}{\partial x}$ and $\frac{\partial N_i}{\partial y}$ from

$$\begin{bmatrix} \frac{\partial N_i}{\partial \alpha} \\ \frac{\partial N_i}{\partial \beta} \end{bmatrix} = \begin{bmatrix} \frac{\partial x}{\partial \alpha} & \frac{\partial y}{\partial \alpha} \\ \frac{\partial x}{\partial \beta} & \frac{\partial y}{\partial \beta} \end{bmatrix} \begin{bmatrix} \frac{\partial N_i}{\partial x} \\ \frac{\partial N_i}{\partial y} \end{bmatrix} = [J] \begin{bmatrix} \frac{\partial N_i}{\partial x} \\ \frac{\partial N_i}{\partial y} \end{bmatrix} \qquad (A3.8)$$

by inverting the Jacobian matrix [J] to obtain

$$\begin{bmatrix} \frac{\partial N_i}{\partial x} \\ \\ \frac{\partial N_i}{\partial y} \end{bmatrix} = [J]^{-1} \begin{bmatrix} \frac{\partial N_i}{\partial \alpha} \\ \\ \frac{\partial N_i}{\partial \beta} \end{bmatrix} \tag{A3.9}$$

One also has

$$ds = dxdy = |J| d\alpha d\beta \tag{A3.10}$$

where $|J|$ is the determinant of $[J]$. Substitution into the local weighted integral expression finally gives an integral of the form

$$\int_{-1}^{1}\int_{-1}^{1} g_j(C_i, \alpha, \beta) d\alpha d\beta \tag{A3.11}$$

Because of the isoparametric transformation this integral can be difficult to evaluate analytically.

A.3.2 Integral Evaluations

The integrals are evaluated here using a Gaussian quadrature numerical integration scheme [A2]. Because the governing differential equation is non-linear, an iteration is used to obtain a solution to the resulting algebraic equation system. This is based on

$$\int_S [\nabla W_j \cdot \tilde{P}^* h^3 \nabla \tilde{P}] dxdy \tag{A3.12}$$

where $\tilde{P}^*$ indicates pressure from a previous iteration. If the elements used are small enough such that $\tilde{P}^*$ and h^3 do not vary appreciably over an element, then the maximum order of polynomial to be integrated is fourth order. This means that the numerical integration scheme itself must be at least fourth order [A2]. Here, to account for an appreciable variation of $\tilde{P}^*$ or h^3 over an element, a sixth order scheme is used (see Figure A5):

$$\int_{-1}^{1}\int_{-1}^{1} g_j(C_i, \alpha, \beta)d\alpha d\beta =$$

$$\sum_{n=1}^{6}\sum_{m=1}^{6} W_{fn}W_{fm}g_j(C_i, \alpha_n, \beta_m) \qquad \text{(A3.13)}$$

Upon performing the summation, one obtains

$$[K_{ji}]_k \quad |P_i|_k \qquad \text{(A3.14)}$$

which represents the contributions to the global algebraic equation system for element "k".

A.3.3 Assembly of Contribution into Global Matrix

To put the element contributions into their appropriate positions in the global matrix, it is necessary to know the connections between local and global nodes. These can be input as data into the computer programme. However, here the elements are arranged such that the connections can be easily generated by the computer for each element.

To illustrate the assembly, consider the case where local nodes "j" and "i" in element "k" are respectively nodes "n" and "m" in the global system. In this case, term K_{ji} is put into the n-th row m-th column position of the global equation system. Contributions from other elements to the n-th row m-th column position are simply added to the element "k" contribution. When all contributions are assembled, one obtains a global equation system of the form

$$[S_{nm}] \; |P_m| = |0| = |R_n| \qquad \text{(A3.15)}$$

A.3.4 Boundary Conditions

For the SailRail problem, boundary conditions are of the specified value type; in other words, pressure is specified at boundary points. For a node "ℓ" where pressure is specified, the ℓ-th row of the global matrix is replaced by

$$S_{\ell\ell} = 1$$

$$S_{\ell k} = 0 \qquad k \neq \ell \qquad \text{(A3.16)}$$

$$R_{\ell} = \text{Boundary pressure}$$

A.3.5 Gauss Seidel Iteration

A successive substitution procedure known as the Gauss Seidel iteration is used to obtain a solution to the global equation system. This is simply

$$P_{\ell} = \left[R_{\ell} - \sum_{\substack{i=1 \\ \ell>1}}^{\ell-1} S_{\ell i} P_i - \sum_{\substack{i=\ell+1 \\ \ell<n}}^{n} S_{\ell i} P_i^* \right] / S_{\ell\ell} \qquad \text{(A3.17)}$$

$$\ell = 1, \ldots, n$$

This procedure makes very efficient use of the space available for array storage. The cycle "ℓ" equal 1 to n with periodic update of the global matrix S is repeated many times, until satisfactory convergence is achieved.

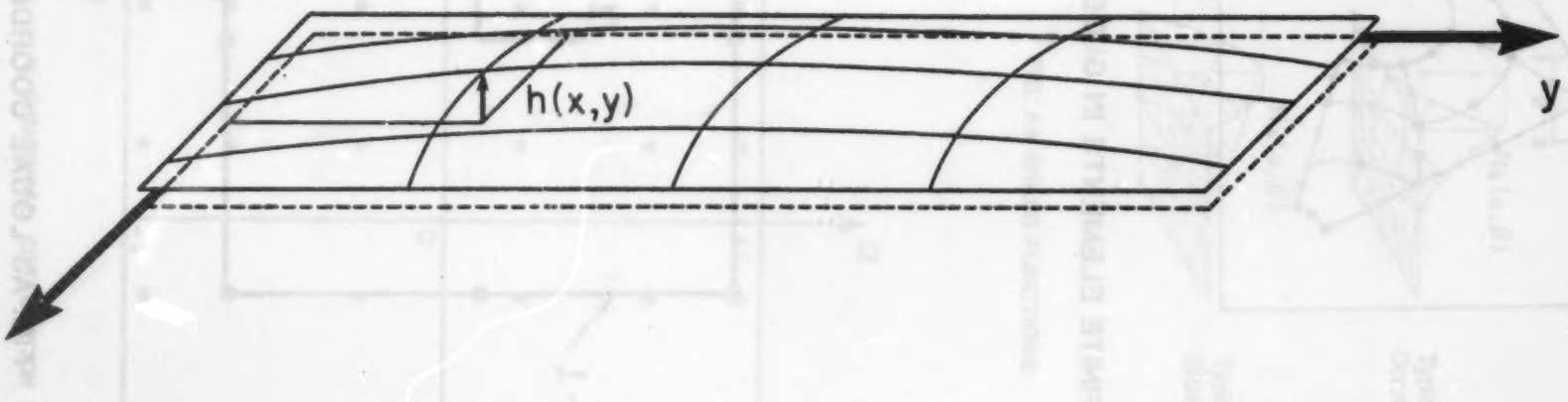

FIG. A1 HYDROSTATIC LUBRICATION GEOMETRY

FIG. A2 FINITE ELEMENTS IN GLOBAL COORDINATE SYSTEM

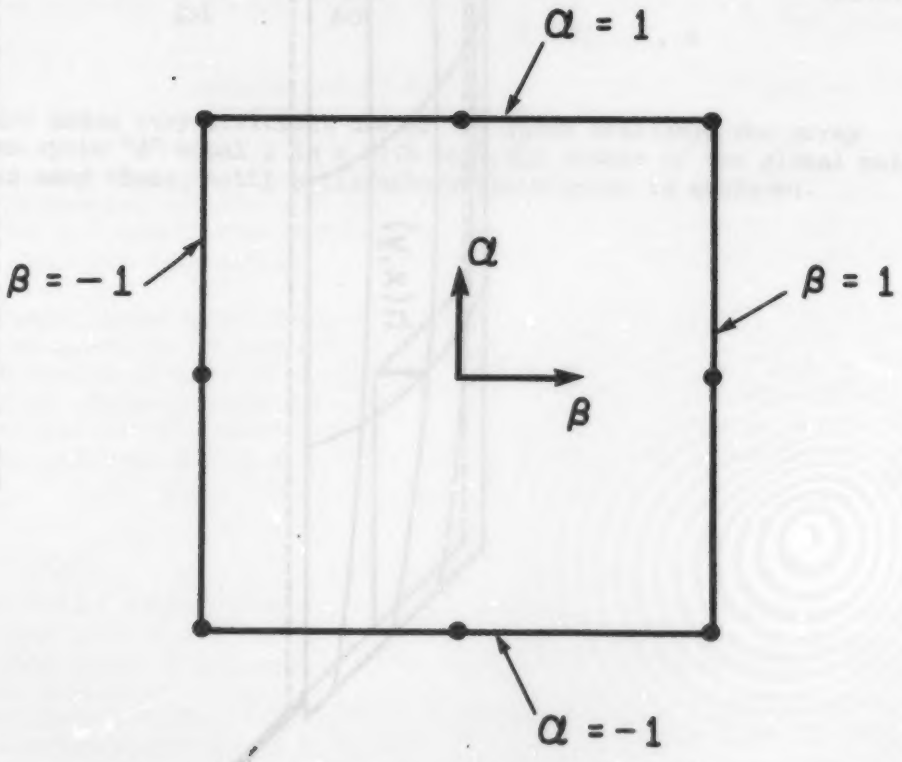

FIG. A3 LOCAL COORDINATE SYSTEM

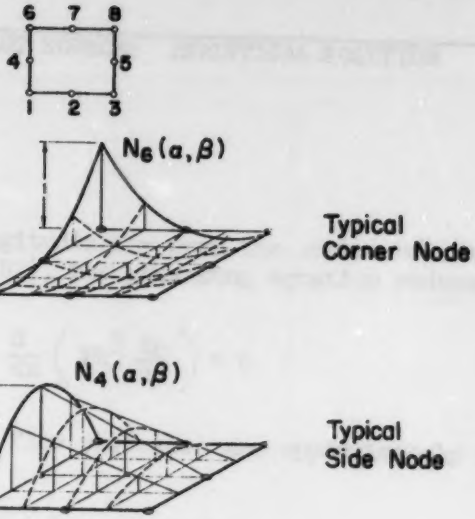

FIG. A4 SHAPE FUNCTIONS

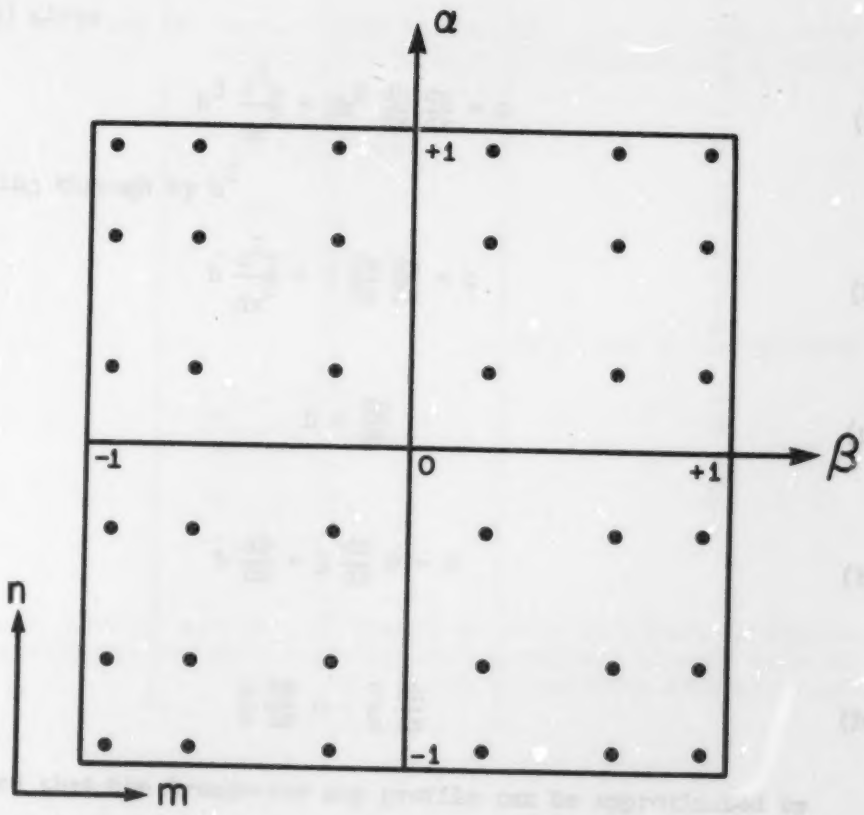

● NUMERICAL INTEGRATION POINTS

FIG. A5 NUMERICAL LINE INTEGRATION SCHEME

For a slot running longitudinally down the centre of a very long shoe-track configuration (Figure B1), the governing equation reduces to

$$\frac{d}{dx}\left(Ph^3 \frac{dp}{dx} \right) = 0 \tag{B1}$$

For low cavity pressures the flow processes are approximately incompressible in which case

$$P \cong \text{constant} \tag{B2}$$

and (B1) reduces to

$$\frac{d}{dx}\left(h^3 \frac{dp}{dx} \right) = 0 \tag{B3}$$

Expanding (B3) gives

$$h^3 \frac{d^2p}{dx^2} + 3h^2 \frac{dh}{dx} \frac{dp}{dx} = 0 \tag{B4}$$

or upon dividing through by h^2

$$h \frac{d^2p}{dx^2} + 3 \frac{dh}{dx} \frac{dp}{dx} = 0 \tag{B5}$$

Letting

$$D = \frac{dp}{dx} \tag{B6}$$

gives

$$h \frac{dD}{dx} + 3 \frac{dh}{dx} D = 0 \tag{B7}$$

or

$$\frac{1}{D} \frac{dD}{dx} = -\frac{3}{h} \frac{dh}{dx} \tag{B8}$$

If it is assumed that the transverse gap profile can be approximated by

$$h = h_o e^{-\lambda x} \tag{B9}$$

then (B8) reduces to

$$\frac{1}{D}\frac{dD}{dx} = 3\lambda \tag{B10}$$

for which the general solution is

$$D = \frac{dp}{dx} = C_I e^{3\lambda x} \tag{B11}$$

Integrating with respect to x gives

$$P = \frac{C_I e^{3\lambda x}}{3\lambda} + C_J \tag{B12}$$

where C_I and C_J are constants of integration. At the slot (x = 0), P = P_s while at the periphery (x = L), P = P_a. Thus

$$P_s = \frac{C_I}{3\lambda} + C_J \tag{B13}$$

$$P_a = \frac{C_I e^{3\lambda L}}{3\lambda} + C_J \tag{B14}$$

Solving for C_I and C_J gives

$$C_I = \frac{3\lambda(P_s - P_a)}{(1 - e^{3\lambda L})} \tag{B15}$$

$$C_J = \frac{P_a - P_s e^{3\lambda L}}{1 - e^{3\lambda L}} \tag{B16}$$

A typical result is given in Figure B2. As can be seen, the calculated pressure profile closely resembles those obtained from the two dimensional finite element analysis with arbitrarily spaced feed holes.

Shoe and Track Infinitely Long

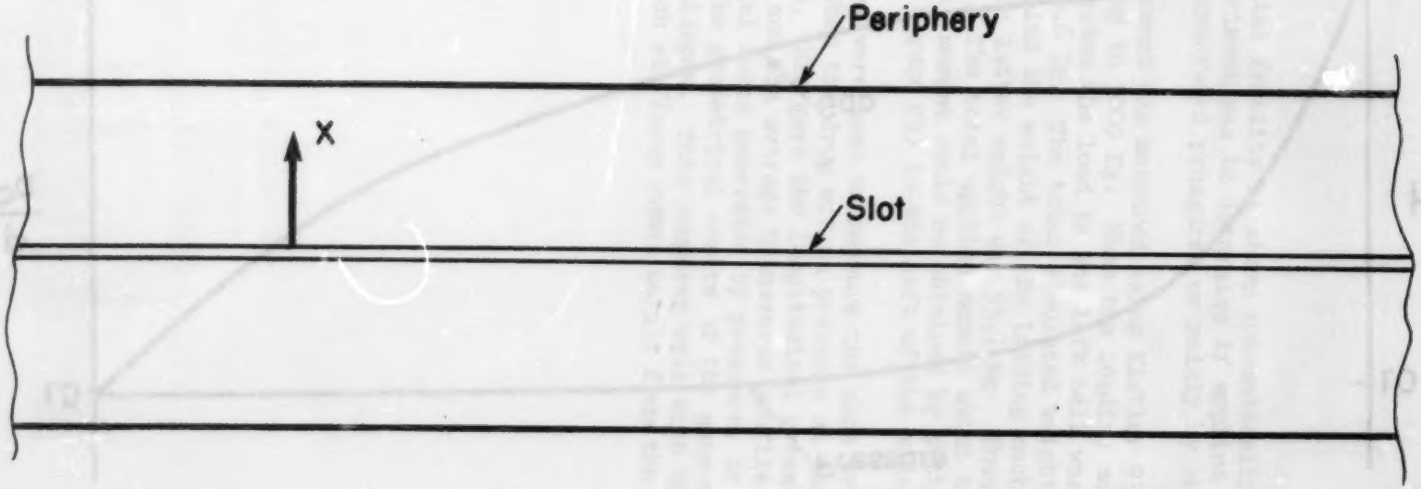

Fig. B1 TRACK WITH LONGITUDINAL SLOT SOURCE

$h_o = 1$
$\lambda = 1$
$P_s = 1.5$ Patm
$P_a = 1.0$ Patm
$L = 3$

Gap $h = h_o e^{-\lambda x}$

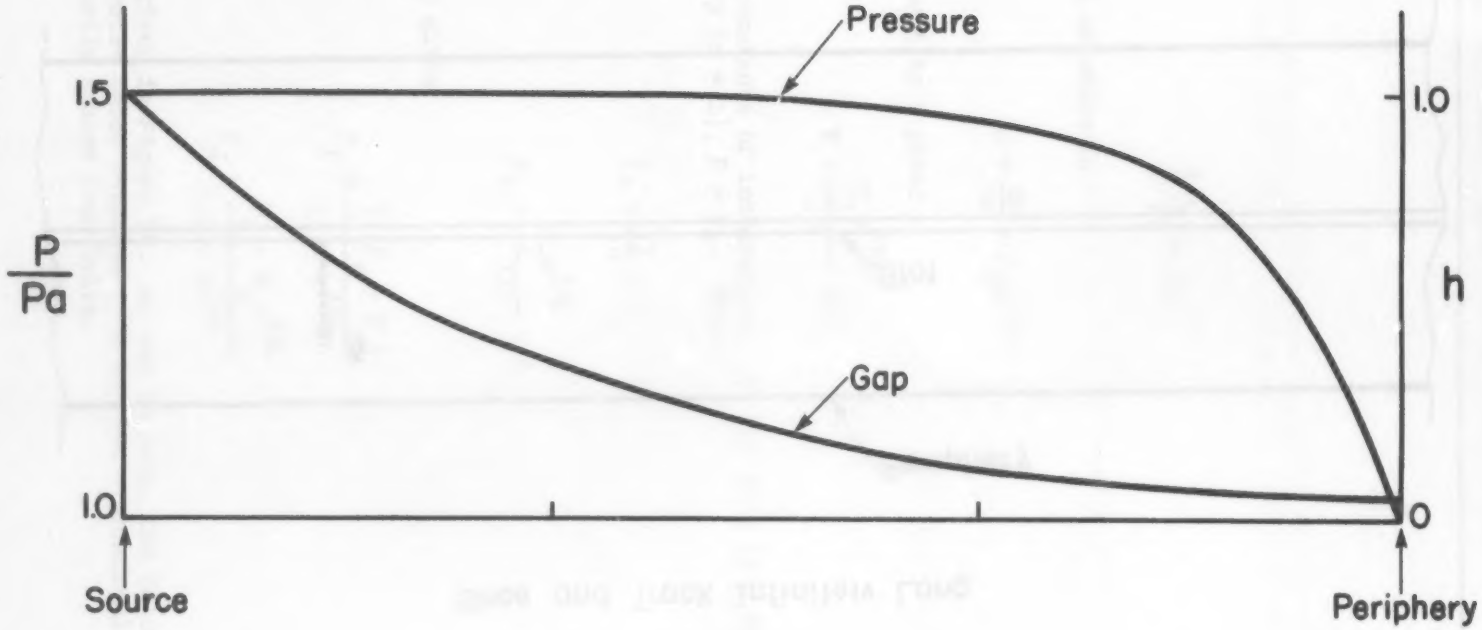

Fig.B2 TYPICAL RESULT FOR LONGITUDINAL SLOT SOURCE

The experimental facility is shown schematically in Figure C1. The purpose of the experiment was to determine if applied moment was counter-balanced mainly by generated pressures or mainly by shoe-track contact.

The applied moment was measured using Kistler 934A load cells capable of measuring loads up to 3000 Kg. When the loading mechanism was pitched 0.20° on the shoe tested the load in the left cell was 196.4 Kg while in the right cell it was 86.6 Kg. The total simulated weight consisted of the sum of these two loads plus the weight of the loading mechanism and a number of its attachments. The latter weight was 53.1 Kg. Thus the total simulated weight was 336.1 Kg. The total applied moment about the midspan was 33.46 Kg-m. Note that this moment could be obtained by putting the total simulated weight 9.97 cm (see Figure C2) to the left of the midspan.

Pressure probes were used to measure the shoe pressure at three longitudinal stations. When the drop off in pressure at the longitudinal ends of the shoe was ignored, this gave the longitudinal pressure distribution given in Figure C3. This and the average transverse profile in Figure C4 gave 328.9 Kg for the total force generated by pressure, or 97.8% of the total simulated weight. The geometrical centre of the generated pressure force was 9.3 cm left of midspan. This compares well with the applied moment position. Thus, the pitch stiffness comes mainly from the generated pressure forces.

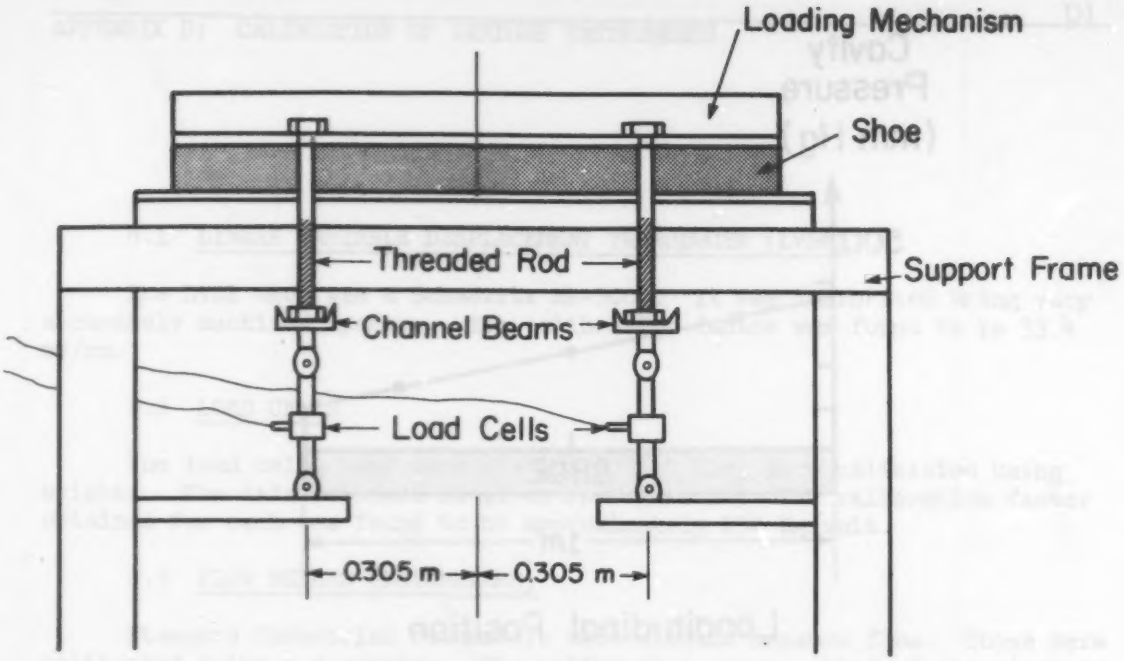

FIG. C1 SCHEMATIC OF STATIC PITCH STIFFNESS FACILITY

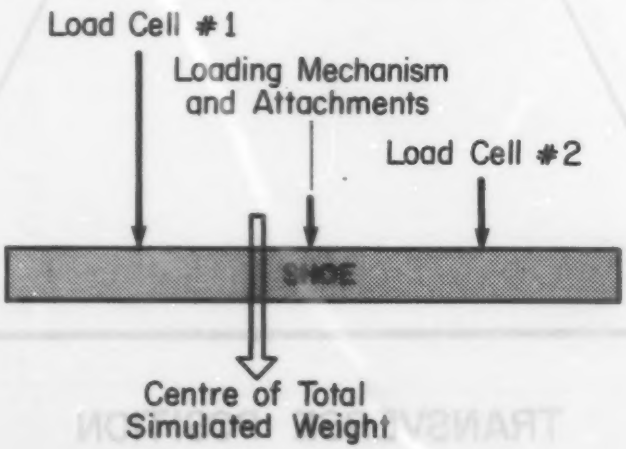

FIG. C2 CENTRE OF TOTAL SIMULATED WEIGHT

FLOW CHART OF MAIN PROGRAMME

HYDROSTATIC LUBRICATION ANALYSIS OF SAILRAIL

```
C
C     GOVERNING DIFFERENTIAL EQUATION:
C     REYNOLDS EQUATION FOR PRESSURE.
C
C
C     A FINITE ELEMENT METHOD IS USED TO REDUCE THE GOVERNING EQUATION
C     TO A SYSTEM OF ALGEBRAIC EQUATIONS.
C
C     A GAUSS SEIDEL ITERATION IS USED TO OBTAIN A SOLUTION.
C
ISN 0002        COMMON/NUM/NP,NE,NBAND,NODE,NIP
ISN 0003        COMMON/NODE/CORD(1500,2),NFIX(1500)
ISN 0004        COMMON/SQUARE/ALPHA(6),WF(6),NOP(500,9)
ISN 0005        COMMON/GAP/H(1500)
ISN 0006        COMMON/PARM/VISL,PATM,PTRACK,HEET
ISN 0007        COMMON/RESULT/P(1500)
ISN 0008        COMMON/MATRIX/GN(1500,27),GM(8,8),F(1500),EF(8),IBP(1800,27)
ISN 0009        COMMON/SAIL/NFLD,NELA,NELB,NELC,NFLD,NI,NJ
ISN 0010        COMMON/PAIL/X(10),Y(13),DX(9),DY(12)
ISN 0011        COMMON/ZER/XZERO(21),YZERO(21),NOPZ(4,8),NZERO(5),MZERO(5)
ISN 0012        COMMON/ONE/XONE(40),YONE(40),ACPO(8,8),NONE(8),MONE(5)
C
C
C     DATA.
ISN 0013        CALL INFO
C
C     STARTING VALUES FOR ITERATION.
ISN 0014        CALL GUESS
C
ISN 0015        I=0
ISN 0016        J=0
ISN 0017        NLIM=5
ISN 0018        NPRINT=5
C
C
C     ITERATION.
ISN 0019     10 CONTINUE
ISN 0020        I=I+1
ISN 0021        J=J+1
C
C     FORMATION OF GLOBAL MATRIX.
ISN 0022        CALL GLOBAL
C
C     SOLUTION BY GAUSS SEIDEL ITERATION.
ISN 0023        CALL SEIDEL
C
ISN 0024        IF(J.EQ.NPRINT) CALL PRINT
```

```
EVEL 2.2.1 (DEC 77,          MAIN          OS/360  FORTRAN H EXTENDED          DATE 80.088/04.04.02      P
ISN 0026        IF(J.EQ.NPRINT) J=0
ISN 0028        IF(I.LT.NLIM) GO TO 10
C
ISN 0030        CALL GRAPH
C
C
ISN 0031        STOP
ISN 0032        END
PTIONS IN EFFECT*NAME(MAIN) OPTIMIZE(2) LINECOUNT(60) SIZE(MAX) AUTODBL(NONE)
PTIONS IN EFFECT*SOURCE EBCDIC NOLIST NODECK OBJECT NOMAP NOFORMAT GOSTMT NOXREF NOALC NOANSF NOTERM FLAG(I)
TATISTICS*      SOURCE STATEMENTS =       31, PROGRAM SIZE =      432, SUBPROGRAM NAME = MAIN
TATISTICS*  NO  DIAGNOSTICS GENERATED
*** END OF COMPILATION ******
                                                        278K BYTES OF CORE NOT USED
```

```
EVEL 2.2.1 (DEC 77)                    OS/360  FORTRAN H EXTENDED          DATE 80.098/14.04.05
QUESTED OPTIONS: OPTIMIZE(2)
TIONS IN EFFECT: NAME(MAIN) OPTIMIZE(2) LINECOUNT(60) SIZE(MAX) AUTODBL(NONE)
                 SOURCE EXDOIC NOLIST NODECK OBJECT NOMAP NOFORMAT GOSTMT NOXREF NOALC NOANSF NOTERM FLAG(I)

ISN 0002              SUBROUTINE  ZERO(I,J)
                    C
                    C
                    C     MACRO-ELEMENT WITHOUT SOURCES.
                    C
                    C
ISN 0003              COMMON/NUM/NP,NE,NBAND,NODE,NIP
ISN 0004              COMMON/MODE/CORD(1500,2),NFIX(1500)
ISN 0005              COMMON/SQUARE/ALPHA(6),WF(6),NOP(500,9)
ISN 0006              COMMON/SAIL/NFLD,NELA,NELB,NELC,NELD,NI,NJ
ISN 0007              COMMON/SAIL/X(10),Y(13),DX(9),DY(12)
ISN 0008              COMMON/ZER/XZERO(21),YZERO(21),NOPZ(4,8),NZERO(5),MZERO(5)
ISN 0009              DIMENSION NHL(21)
                    C
                    C
ISN 0010              DO 10 K=1,21
ISN 0011              IF(K.LE.5)
                     *NHL(K)=NFLD+K-1
ISN 0013               IF(K.GT.5.AND.K.LE.8)
                     *NHL(K)=NELA+K-6
ISN 0015               IF(K.GT.8.AND.K.LE.13)
                     *NHL(K)=NELB+K-9
ISN 0017               IF(K.GT.12.AND.K.LE.16)
                     *NHL(K)=NELC+K-14
ISN 0019               IF(K.GT.16)
                     *NHL(K)=NELD+K-17
ISN 0021           10  CONTINUE
ISN 0022              DO 50 N=1,4
ISN 0023              NOP(NE+N,9)=0
ISN 0024              DO 50 M=1,8
ISN 0025              NOP(NE+N,M)=NHL(NOPZ(N,M))
ISN 0026           50 CONTINUE
ISN 0027              NE=NE+4
ISN 0028              KKO=4
ISN 0029              IF(J.EQ.NJ) KKO=5
ISN 0031              DO 100 KK=1,KKO
ISN 0032              KO=MZERO(KK)-1
ISN 0033              IF(I.EQ.NI) KO=MZERO(KK)
ISN 0035              KS=NZERO(KK)
ISN 0036              DO 100 K=KS,KO
ISN 0037              NIT=NHL(K)
ISN 0038              CORD(NIT,1)=X(I)+XZERO(K)*DX(I)
ISN 0039              CORD(NIT,2)=Y(J)+YZERO(K)*DY(J)
ISN 0040              NFIX(NIT)=0
ISN 0041              IF(J.EQ.1.AND.K.LT.5) NFIX(NIT)=2
ISN 0043              IF(J.EQ.1.AND.K.LT.5) GO TO 100
ISN 0045              IF(J.EQ.NJ.AND.K.LT.21.AND.K.GE.17) NFIX(NIT)=2
ISN 0047              IF(J.EQ.NJ.AND.K.LT.21.AND.K.GE.17) GO TO 100
ISN 0049              IF(I.EQ.1.AND.K.EQ.KS) NFIX(NIT)=2
ISN 0051              IF(I.EQ.1.AND.K.EQ.KS) GO TO 100
ISN 0053              IF(I.EQ.NI.AND.K.EQ.KO) NFIX(NIT)=2
ISN 0055           100 CONTINUE
                    C

EVEL 2.2.1 (DEC 77)                ZERO          OS/360  FORTRAN H EXTENDED          DATE 80.098/14.04.05
                    C
ISN 0056              RETURN
ISN 0057              END
PTIONS IN EFFECT*NAME(MAIN) OPTIMIZE(2) LINECOUNT(60) SIZE(MAX) AUTODBL(NONE)
PTIONS IN EFFECT*SOURCE EXDOIC NOLIST NODECK OBJECT NOMAP NOFORMAT GOSTAT NOXREF NOALC NOANSF NOTERM FLAG(I)
TATISTICS*      SOURCE STATEMENTS =      56, PROGRAM SIZE =     1334, SUBPROGRAM NAME =  ZERO
TATISTICS*  NO  DIAGNOSTICS GENERATED
**** END OF COMPILATION *****                                  270K BYTES OF CORE NOT USED
```

```
EVEL 2.2.1 (DEC 77)                    OS/360  FORTRAN H EXTENDED          DATE 80.088/04.04.07      P
QUESTED OPTIONS: OPTIMIZE(2)
TIONS IN EFFECT: NAME(MAIN) OPTIMIZE(2) LINECOUNT(60) SIZE(MAX) AUTODBL(NONE)
                 SOURCE EBCDIC NOLIST NODECK OBJECT NOMAP NOFORMAT GOSTMT NOXREF NOALC NOANSF NOTERM FLAG(I)
ISN 0002              SUBROUTINE ONE(I,J)
                      C
                      C
                      C     MACRO-ELEMENT WITH ONE PRESSURE SOURCE.
                      C
                      C
ISN 0003              COMMON/NUM/NP,NE,NBAND,NOCE,NIB
ISN 0004              COMMON/MODE/CORD(1500,2),NFIX(1500)
ISN 0005              COMMON/SQUARE/ALPHA(6),WF(6),NOP(500,9)
ISN 0006              COMMON/SAIL/NFLD,NELA,NELB,NELC,NFLD,NI,NJ
ISN 0007              COMMON/RAIL/X(10),Y(13),DX(9),DY(12)
ISN 0008              COMMON/ON/XONE(40),YONE(40),NOPO(8,8),NONE(5),MONE(5)
ISN 0009              DIMENSION NHL(40)
                      C
                      C
ISN 0010              DO 10 K=1,40
ISN 0011              IF(K.LE.5)
                     *NHL(K)=NFLD+K-1
ISN 0013              IF(K.GT.6.AND.K.LE.10)
                     *NHL(K)=NELA+K-6
ISN 0015              IF(K.GT.10.AND.K.LE.30)
                     *NHL(K)=NELB+K-11
ISN 0017              IF(K.GT.30.AND.K.LE.35)
                     *NHL(K)=NELC+K-31
ISN 0019              IF(K.GT.35)
                     *NHL(K)=NELD+K-36
ISN 0021           10 CONTINUE
ISN 0022              DO 50 N=1,8
ISN 0023              NOP(NF+N,9)=1
ISN 0024              DO 50 M=1,8
ISN 0025              NOP(NF+N,M)=NHL(NOPO(N,M))
ISN 0026           50 CONTINUE
ISN 0027              NF=NF+8
ISN 0028              KK=6
ISN 0029              DO 100 KK=1,KK2
ISN 0030              KS=NONE(KK)-1
ISN 0031              KJ=NONE(KK)
ISN 0032              DO 100 K=KS,KJ
ISN 0033              NIT=NHL(K)
ISN 0034              CORD(NIT,1)=X(I)+XONE(K)*DX(I)
ISN 0035              CORD(NIT,2)=Y(J)+YONE(K)*DY(J)
ISN 0036              NFIX(NIT)=0
ISN 0037              IF(K.GE.13.AND.K.LE.28) NFIX(NIT)=1
ISN 0038          100 CONTINUE
                      C
                      C
ISN 0040              RETURN
ISN 0041              END

PTIONS IN EFFECT: NAME(MAIN) OPTIMIZE(2) LINECOUNT(60) SIZE(MAX) AUTODBL(NONE)

PTIONS IN EFFECT: SOURCE EBCDIC NOLIST NODECK OBJECT NOMAP NOFORMAT GOSTMT NOXREF NOALC NOANSF NOTERM FLAG(I)

TATISTICS*      SOURCE STATEMENTS =      40, PROGRAM SIZE =     1156, SUBPROGRAM NAME =   ONE

EVEL 2.2.1 (DEC 77)                    OS/360  FORTRAN H EXTENDED          DATE 80.088/04.04.07      P
TATISTICS*  NO  DIAGNOSTICS GENERATED
**** END OF COMPILATION ****                                  274K BYTES OF CORE NOT USED
```

```
EVEL 2.2.1 (DEC 77)                    OS/360  FORTRAN H EXTENDED          DATE 80.098/04.04.08          3
QUESTED OPTIONS: OPTIMIZE(2)
TIONS IN EFFECT: NAME(MAIN) OPTIMIZE(2) LINECOUNT(60) SIZE(MAX) AUTODBL(NONE)
                 SOURCE EBCDIC NOLIST NODECK OBJECT NOMAP NOFORMAT GOSTMT NOXREF NOALC NOANSF NOTERM FLAG(I)

 ISN 0002              SUBROUTINE GUESS
                C
                C     STARTING VALUES FOR ITERATION.
                C
                C
 ISN 0003              COMMON/NUM/NP,NE,NBAND,NODE,NIP
 ISN 0004              COMMON/PARM/VISL,PATM,PTRACK,HSET
 ISN 0005              COMMON/RESULT/P(1500)
                C
                C
 ISN 0006              DO 10 I=1,NP
 ISN 0007              P(I)=PTRACK
 ISN 0008           10 CONTINUE
                C
                C
 ISN 0009              RETURN
 ISN 0010              END
PTIONS IN EFFECT*NAME(MAIN) OPTIMIZE(2) LINECOUNT(60) SIZE(MAX) AUTODBL(NONE)
PTIONS IN EFFECT*SOURCE EBCDIC NOLIST NODECK OBJECT NOMAP NOFORMAT GOSTMT NOXREF NOALC NOANSF NOTERM FLAG(I)
TATISTICS*      SOURCE STATEMENTS =      9, PROGRAM SIZE =     246, SUBPROGRAM NAME = GUESS
TATISTICS*  NO  DIAGNOSTICS GENERATED
**** END OF COMPILATION *****                                  282K BYTES OF CORE NOT USED
```

```
EVEL 2.2.1 (DEC 77)                    OS/360  FORTRAN H EXTENDED          DATE 80.098/04.04.10          PAG
QUESTED OPTIONS: OPTIMIZE(2)
TIONS IN EFFECT: NAME(MAIN) OPTIMIZE(2) LINECOUNT(60) SIZE(MAX) AUTODBL(NONE)
                 SOURCE EBCDIC NOLIST NODECK OBJECT NOMAP NOFORMAT GOSTMT NOXREF NOALC NOANSF NOTERM FLAG(I)

 ISN 0002              SUBROUTINE PRINT
                C
                C     OUTPUT.
                C
 ISN 0003              COMMON/NUM/NP,NE,NBAND,NODE,NIP
 ISN 0004              COMMON/MODE/CORD(1500,2),NPIX(1500)
 ISN 0005              COMMON/GAP/H(1500)
 ISN 0006              COMMON/RESULT/P(1500)
                C
                C
 ISN 0007              WRITE(6,10)
 ISN 0008           10 FORMAT('1',/,10X,'PRESSURE PROFILES')
 ISN 0009              DO 1000 I=1,NP
 ISN 0010              WRITE(6,100) I,NPIX(I),P(I),H(I),CORD(I,1),CORD(I,2)
 ISN 0011         1000 CONTINUE
 ISN 0012          100 FORMAT(10X,2I3,10X,4(E12.5,5X))
                C
                C
 ISN 0013              RETURN
 ISN 0014              END
PTIONS IN EFFECT*NAME(MAIN) OPTIMIZE(2) LINECOUNT(60) SIZE(MAX) AUTODBL(NONE)
PTIONS IN EFFECT*SOURCE EBCDIC NOLIST NODECK OBJECT NOMAP NOFORMAT GOSTMT NOXREF NOALC NOANSF NOTERM FLAG(I)
TATISTICS*      SOURCE STATEMENTS =     13, PROGRAM SIZE =     430, SUBPROGRAM NAME = PRINT
TATISTICS*  NO  DIAGNOSTICS GENERATED
**** END OF COMPILATION *****                                  282K BYTES OF CORE NOT USED
```

```
VEL 2.2.1 (DEC 77)                    OS/360  FORTRAN H EXTENDED          DATE 80.098/04.04.12        PA
UESTED OPTIONS: OPTIMIZE(2)

IONS IN EFFECT: NAME(MAIN) OPTIMIZE(2) LINECOUNT(60) SIZE(MAX) AUTODBL(NONE)
                SOURCE EBCDIC NOLIST NODECK OBJECT NOMAP NOFORMAT GOSTMT NOXREF NOALC NOANSF NOTERM FLAG(I)

ISN 0002.             SUBROUTINE GLOBAL
                C
                C     ------------------------------------------------------------------
                C
                C     FORMATION OF GLOBAL MATRIX.
                C
                C     ------------------------------------------------------------------
ISN 0003              COMMON I/NUM/NP,NE,NDAND,NODE,NIP
ISN 0004              COMMON/NODE/CORD(1500,2),NFIX(1500)
ISN 0005              COMMON/SQUARE/ALPHA(6),WF(6),NOP(500,9)
ISN 0006              COMMON/GAP/H(1500)
ISN 0007              COMMON/PASN/VISL,PATM,PTRACK,NSET
ISN 000F              COMMON/RESULT/P(1500)
ISN 0009              COMMON/MATRIX/GM(1500,27),EM(8,8),F(1500),ER(8),ISP(1500,27)
                C
                C     ------------------------------------------------------------------
ISN 0010              DO 1 I=1,NP
ISN 0011              DO 2 J=1,NDAND
ISN 0012              GM(I,J)=0.0
ISN 0013              ISP(I,J)=0
ISN 0014            2 CONTINUE
ISN 0015              ISP(I,1)=I
ISN 0016              F(I)=0.0
ISN 0017            1 CONTINUE
                C     ------------------------------------------------------------------
ISN 0018              DO 10 N=1,NE
ISN 0019              CALL LOCAL(N)
ISN 0020              DO 10 I=1,NODE
ISN 0021              NROW=NOP(N,I)
ISN 0022              DO 20 J=1,NODE
ISN 0023              NCOL=NOP(N,J)
ISN 0024              DO 5 M=1,NDAND
ISN 0025              IF(ISP(NROW,M)-NCOL) 6,7,6
ISN 0026            6 IF(ISP(NROW,M)) 8,8,5
ISN 0027            5 CONTINUE
ISN 0028            8 CONTINUE
ISN 0029              ISP(NROW,M)=NCOL
ISN 0030            7 CONTINUE
ISN 0031              GM(NROW,M)=GM(NROW,M)+EM(I,J)
ISN 0032           20 CONTINUE
ISN 0033              F(NROW)=F(NROW)+ER(I)
ISN 0034           10 CONTINUE
                C     ------------------------------------------------------------------
ISN 0035              DO 50 I=1,NP
ISN 0036              IF(NFIX(I).EQ.0) GO TO 50
ISN 0038              IF(NFIX(I).EQ.1) FC=PTRACK
ISN 0040              IF(NFIX(I).EQ.2) FC=PATM
ISN 0042              DO 45 J=2,NDAND
ISN 0043              GM(I,J)=0.0
ISN 0044           45 CONTINUE
ISN 0045              GM(I,1)=1.0
ISN 0046              F(I)=FC
ISN 0047           50 CONTINUE
                C     ------------------------------------------------------------------

VEL 2.2.1 (DEC 77)          GLOBAL          OS/360  FORTRAN H EXTENDED          DATE 80.098/04.04.12        PA
                C     ------------------------------------------------------------------
ISN 0048              RETURN
ISN 0049              END
TIONS IN EFFECT: NAME(MAIN) OPTIMIZE(2) LINECOUNT(60) SIZE(MAX) AUTODBL(NONE)
TIONS IN EFFECT: SOURCE EBCDIC NOLIST NODECK OBJECT NOMAP NOFORMAT GOSTMT NOXREF NOALC NOANSF NOTERM FLAG(I)
ATISTICS:      SOURCE STATEMENTS =     48, PROGRAM SIZE =     1100, SUBPROGRAM NAME =GLOBAL
ATISTICS:  NO  DIAGNOSTICS GENERATED
*** END OF COMPILATION ***:***                                  276K BYTES OF CORE NOT USED
```

```
EVEL 2.2.1 (DEC 77)                    OS/360  FORTRAN H EXTENDED          DATE 80.088/04.04.14
QUESTED OPTIONS: OPTIMIZE(2)
TIONS IN EFFECT: NAME(MAIN) OPTIMIZE(2) LINECOUNT(60) SIZE(MAX) AUTODBL(NONE)
                 SOURCE EBCDIC NOLIST NODECK OBJECT NOMAP NOFORMAT GOSTMT NOXREF NOALC NOANSF NOTERM FLAG(I

ISN 0002            SUBROUTINE SEIDEL
                    C
                    C
                    C     SOLUTION BY GAUSS SEIDEL ITERATION.
                    C
                    C
ISN 0003            COMMON/NUM/NP,NE,NBAND,NODE,NIP
ISN 0004            COMMON/RESULT/P(1500)
ISN 0005            COMMON/MATRIX/GM(1500,27),EM(8,8),F(1500),ER(8),ISP(1500,27)
ISN 0006            DIMENSION POLD(1500)
                    C
                    C
                    C     RELAXATION COEFFICIENT.
ISN 0007            RELAX=1.0
                    C
                    C     NUMBER OF OFF-DIAGONAL TERMS.
ISN 0008            DO 1 N=1,NP
ISN 0009            DO 2 M=1,NBAND
ISN 0010            IF(ISP(N,M).NE.0) GO TO 2
ISN 0012            ISP(N,1)=M-1
ISN 0013            GO TO 1
ISN 0014          2 CONTINUE
ISN 0016          1 CONTINUE
                    C
                    C     NUMBER OF CYCLES.
ISN 0016            NMAX=1000
                    C
                    C     STORING ESTIMATE OF PRESSURE.
ISN 0017            DO 10 N=1,NP
ISN 0018            POLD(N)=P(N)
ISN 0019         10 CONTINUE
                    C
                    C     LOOP ON CYCLES.
ISN 0020            DO 500 NLOOP=1,NMAX
                    C     LOOP ON EQUATIONS.
ISN 0021            DO 700 N=1,NP
ISN 0022            FX=F(N)
ISN 0023            MOM=ISP(N,1)
ISN 0024            DO 737 M=2,MOM
ISN 0025            L=ISP(N,M)
ISN 0026            FX=FX-GM(N,M)*P(L)
ISN 0027        707 CONTINUE
ISN 0028            DOG=FX/GM(N,1)
ISN 0029            P(N)=POLD(N)*(1.-RELAX)+RELAX*DOG
ISN 0030        700 CONTINUE
ISN 0031        500 CONTINUE
                    C
                    C
ISN 0032            RETURN
ISN 0033            END
PTIONS IN EFFECT*NAME(MAIN) OPTIMIZE(2) LINECOUNT(60) SIZE(MAX) AUTODBL(NONE)
PTIONS IN EFFECT*SOURCE EBCDIC NOLIST NODECK OBJECT NOMAP NOFORMAT GOSTMT NOXREF NOALC NOANSF NOTERM FLAG(I

EVEL 2.2.1 (DEC 77)                    OS/360  FORTRAN H EXTENDED          DATE 80.088/04.04.14
TATISTICS*     SOURCE STATEMENTS =     32, PROGRAM SIZE =     6706, SUBPROGRAM NAME =SEIDEL
TATISTICS*   NO  DIAGNOSTICS GENERATED
**** END OF COMPILATION ****                                  282K BYTES OF CORE NOT USED
```

```
EVEL 2.2.1 (DEC 77)                    OS/360  FORTRAN H EXTENDED              DATE 80.098/04.04.16          PA
QUESTED OPTIONS: OPTIMIZE(2)
TIONS IN EFFECT: NAME(MAIN) OPTIMIZE(2) LINECOUNT(60) SIZE(MAX) AUTODBL(NONE)
                 SOURCE EXDCIC NOLIST NODECK OBJECT NOMAP NOFORMAT COSTMT NOXREF NOALC NOANSF NOTERM FLAG(I)
ISN 0002              SUBROUTINE LOCAL(N)
                      C
                      C
                      C     ELEMENT CONTRIBUTIONS TO GLOBAL MATRIX.
                      C
ISN 0003              COMMON/NUM/NP,NE,NDAND,NODE,NIP
ISN 0004              COMMON/NODE/CORD(1500,2),NFIX(1500)
ISN 0005              COMMON/SQUARE/ALPHA(6),WF(6),NOP(500,6)
ISN 0006              COMMON/GAP/H(1500)
ISN 0007              COMMON/PARM/VISL,DATN,PTRACK,NSET
ISN 0008              COMMON/RESULT/P(1500)
ISN 0009              COMMON/MATRIX/GM(1500,27),EM(8,8),F(1500),ER(8),ISP(1500,27)
ISN 0010              DIMENSION SF(8,6,6),DEFA(8,6,6),DEFB(8,6,6)
ISN 0011              DIMENSION DXDA(6,6),DXDB(6,6),DYDA(6,6),DYDB(6,6)
ISN 0012              DIMENSION DETJ(6,6),DJII(6,6),DJIJ(6,6),DJJI(6,6),DJJJ(6,6)
                      C
                      C
ISN 0013              DO 10 I=1,NIP
ISN 0014              A=ALPHA(I)
ISN 0015              DO 10 J=1,NIP
ISN 0016              B=ALPHA(J)
ISN 0017              SF(1,I,J)=1./4.*(1.-A)*(1.-B)*(-A-B-1.)
ISN 0018              SF(3,I,J)=1./4.*(1.-A)*(1.+B)*(-A+B-1.)
ISN 0019              SF(5,I,J)=1./4.*(1.+A)*(1.-B)*(A-B-1.)
ISN 0020              SF(8,I,J)=1./4.*(1.+A)*(1.+B)*(A+B-1.)
ISN 0021              SF(4,I,J)=1./2.*(1.-A*A)*(1.-B)
ISN 0022              SF(6,I,J)=1./2.*(1.-A*A)*(1.+B)
ISN 0023              SF(2,I,J)=1./2.*(1.-A)*(1.-B*B)
ISN 0024              SF(7,I,J)=1./2.*(1.+A)*(1.-B*B)
ISN 0025              DEFA(1,I,J)=1./4.*(1.-B)*((-A-B-1.)+(1.-A))
ISN 0026              DEFB(1,I,J)=1./4.*(1.-A)*((-A-B-1.)+(1.-B))
ISN 0027              DEFA(3,I,J)=1./4.*(1.+B)*((-A+B-1.)+(1.-A))
ISN 0028              DEFB(3,I,J)=1./4.*(1.-A)*((-A+B-1.)+(1.+B))
ISN 0029              DEFA(5,I,J)=1./4.*(1.-B)*((A-B-1.)+(1.+A))
ISN 0030              DEFB(5,I,J)=1./4.*(1.+A)*((A-B-1.)+(1.-B))
ISN 0031              DEFA(8,I,J)=1./4.*(1.+B)*((A+B-1.)+(1.+A))
ISN 0032              DEFB(8,I,J)=1./4.*(1.+A)*((A+B-1.)+(1.+B))
ISN 0033              DEFA(4,I,J)=-A*(1.-B)
ISN 0034              DEFB(4,I,J)=-1./2.*(1.-A*A)
ISN 0035              DEFA(6,I,J)=-A*(1.+B)
ISN 0036              DEFB(6,I,J)=1./2.*(1.-A*A)
ISN 0037              DEFA(2,I,J)=-1./2.*(1.-B*B)
ISN 0038              DEFB(2,I,J)=-B*(1.-A)
ISN 0039              DEFA(7,I,J)=1./2.*(1.-B*B)
ISN 0040              DEFB(7,I,J)=-B*(1.+A)
ISN 0041           10 CONTINUE
ISN 0042              DO 1 I=1,NODE
ISN 0043              DO 2 J=1,NODE
ISN 0044              EM(I,J)=0.0
ISN 0045            2 CONTINUE
ISN 0046              ER(I)=0.0
ISN 0047            1 CONTINUE
```

```
EVEL 2.2.1 (DEC 77)                    LOCAL          OS/360  FORTRAN H EXTENDED              DATE 80.098/04.04.16          PA
                      C
ISN 0048              DO 100 I=1,NIP
ISN 0049              DO 100 J=1,NIP
ISN 0050              DXDA(I,J)=0.0
ISN 0051              DXDB(I,J)=0.0
ISN 0052              DYDA(I,J)=0.0
ISN 0053              DYDB(I,J)=0.0
ISN 0054          100 CONTINUE
ISN 0055              DO 500 K=1,NODE
ISN 0056              M=NOP(N,K)
ISN 0057              DO 500 I=1,NIP
ISN 0058              DO 500 J=1,NIP
ISN 0059              DXDA(I,J)=DXDA(I,J)+DEFA(K,I,J)*CORD(M,1)
ISN 0060              DXDB(I,J)=DXDB(I,J)+DEFB(K,I,J)*CORD(M,1)
ISN 0061              DYDA(I,J)=DYDA(I,J)+DEFA(K,I,J)*CORD(M,2)
ISN 0062              DYDB(I,J)=DYDB(I,J)+DEFB(K,I,J)*CORD(M,2)
ISN 0063          500 CONTINUE
ISN 0064              DO 1000 I=1,NIP
ISN 0065              DO 1000 J=1,NIP
ISN 0066              DETJ(I,J)=DYDA(I,J)*DXDB(I,J)-DXDA(I,J)*DYDB(I,J)
ISN 0067              DJII(I,J)=DXDB(I,J)/DETJ(I,J)
ISN 0068              DJIJ(I,J)=-DXDA(I,J)/DETJ(I,J)
ISN 0069              DJJI(I,J)=-DYDB(I,J)/DETJ(I,J)
ISN 0070              DJJJ(I,J)=DYDA(I,J)/DETJ(I,J)
ISN 0071         1000 CONTINUE
ISN 0072              DO 20 M=1,NODE
ISN 0073              DO 20 I=1,NIP
ISN 0074              DO 20 J=1,NIP
ISN 0075              WEF(M,I,J)
ISN 0076              WFO=WF(I)*WF(J)
ISN 0077              DWX=DEFA(M,I,J)*DJJI(I,J)+DEFB(M,I,J)*DJJJ(I,J)
ISN 0078              DWY=DEFA(M,I,J)*DJIJ(I,J)+DEFB(M,I,J)*DJIJ(I,J)
ISN 0079              HO=0.0
ISN 0080              PO=0.0
ISN 0081              DO 25 K=1,NODE
ISN 0082              MM=NOP(N,K)
ISN 0083              HO=HO+SF(K,I,J)*H(MM)
ISN 0084              PO=PO+SF(K,I,J)*P(MM)
ISN 0085           25 CONTINUE
ISN 0086              FO=PO*HO*HO*HO/12.0/VISL*DETJ(I,J)*WFO
ISN 0087              DO 50 K=1,NODE
ISN 0088              DFX=DEFA(K,I,J)*DJJI(I,J)+DEFB(K,I,J)*DJJJ(I,J)
ISN 0089              DFY=DEFA(K,I,J)*DJII(I,J)+DEFB(K,I,J)*DJIJ(I,J)
ISN 0090              EM(M,K)=EM(M,K)+(DWX*DFX+DWY*DFY)*FO
ISN 0091           50 CONTINUE
ISN 0092           20 CONTINUE
                      C
ISN 0093              RETURN
ISN 0094              END
PTIONS IN EFFECT*NAME(MAIN) OPTIMIZE(2) LINECOUNT(60) SIZE(MAX) AUTODBL(NONE)
PTIONS IN EFFECT*SOURCE EXDCIC NOLIST NODECK OBJECT NOMAP NOFORMAT COSTMT NOXREF NOALC NOANSF NOTERM FLAG(I)
TATISTICS*     SOURCE STATEMENTS =      93, PROGRAM SIZE =     7326, SUBPROGRAM NAME = LOCAL
TATISTICS*  NO  DIAGNOSTICS GENERATED
```

```
EVEL 2.2.1 (DEC 77)          LOCAL          OS/360  FORTRAN H EXTENDED          DATE 80.088/14.04.16          3A
**** END OF COMPILATION *******                          250K BYTES OF CORE NOT USED
```

```
EVEL 2.2.1 (DEC 77)                    OS/360  FORTRAN H EXTENDED          DATE 80.088/14.04.18          3A
QUESTED OPTIONS: OPTIMIZE(2)
TIONS IN EFFECT: NAME(MAIN) OPTIMIZE(2) LINECOUNT(60) SIZE(MAX) AUTODBL(NONE)
                 SOURCE EBCDIC NOLIST NODECK OBJECT NOMAP NOFORMAT COSTMY NOXREF NOALC NOANSF NOTERM FLAG(I)

ISN 0002                SUBROUTINE GRAPH
                C
                C
                C       PRESSURE 3-D PLOT.
                C
ISN 0003                COMMON/NUM/NP,NE,NUAND,NODE,NIP
ISN 0004                COMMON/MODE/CORD(1500,2),NFIX(150C)
ISN 0005                COMMON/GAP/H(1500)
ISN 0006                COMMON/PARM/VISL,PATM,PTRACK,MSET
ISN 0007                COMMON/RESULT/P(1500)
ISN 0008                DIMENSION XOC(5),YOC(5)
ISN 0009                DIMENSION PX(1500),PY(1500),HX(1500),HY(1500)
ISN 0010                DIMENSION NT(100)
                C
                C
ISN 0011                PI=3.1415
ISN 0012                DELX=.15
ISN 0013                DELY=.025
ISN 0014                CON=40.
                C
ISN 0015                CALL PLOTST('4JH-SAILRAIL',12)
ISN 0016                CALL FACTOR(0.333)
ISN 0017                CALL PLOT(1.,1.,-3)
ISN 0018                CALL LINEWT(-1)
ISN 0019                CALL SYMBOL(0.,.50,0.50,8HPRESSURE,0.0,8)
ISN 0020                XOC(1)=DELX
ISN 0021                YOC(1)=DELY
ISN 0022                XOC(2)=XOC(1)-0.15*COS(PI/4.)
ISN 0023                YOC(2)=YOC(1)+0.15*SIN(PI/4.)
ISN 0024                XOC(3)=XOC(2)+0.6*COS(PI/18.)
ISN 0025                YOC(3)=YOC(2)+0.6*SIN(PI/18.)
ISN 0026                XOC(4)=XOC(3)+0.15*SIN(PI/4.)
ISN 0027                YOC(4)=YOC(3)-0.15*COS(PI/4.)
ISN 0028                XOC(5)=XOC(1)
ISN 0029                YOC(5)=YOC(1)
ISN 0030                DO 1 I=1,5
ISN 0031                XOC(I)=CON*XOC(I)
ISN 0032                YOC(I)=CON*YOC(I)
ISN 0033              1 CONTINUE
ISN 0034                CALL PLOT(XOC(1),YOC(1),3)
ISN 0035                CALL LINEWT(-2)
ISN 0036                DO 2 I=2,5
ISN 0037                CALL PLOT(XOC(I),YOC(I),2)
ISN 0038              2 CONTINUE
ISN 0039                CALL LINEWT(0)
ISN 0040                DO 10 I=1,NP
ISN 0041                XP=CORD(I,2)*COS(PI/18.)-CORD(I,1)*SIN(PI/4.)+DELX
ISN 0042                YP=CORD(I,2)*SIN(PI/18.)+CORD(I,1)*COS(PI/4.)+DELY
ISN 0043                PX(I)=XP*CON
ISN 0044                PY(I)=((P(I)-PATM)/PATM/5.0+YP)*CON
ISN 0045             10 CONTINUE
ISN 0046                IS0
```

```
EVEL 2.2.1 (DEC 77)          GRAPH          OS/360  FORTRAN H EXTENDED
 ISN 0047              DO 20 I=1,NP
 ISN 0048              YP=CORD(I,1)-.0001
 ISN 0049              IF(YP.LT.0.0) J=J+1
 ISN 0050              IF(YP.LT.0.0) NT(J)=I
 ISN 0053           20 CONTINUE
 ISN 0054              KKK=0
 ISN 0055              NT(J+1)=NP+1
 ISN 0056              DO 50 K=1,J
 ISN 0057              NPOINT=NT(K+1)-NT(K)
 ISN 0058              DO 25 KK=1,NPOINT
 ISN 0059              KKK=KKK+1
 ISN 0060              PXL=PX(KKK)
 ISN 0061              PYL=PY(KKK)
 ISN 0062              CALL PLOT(PXL,PYL,2)
 ISN 0063           25 CONTINUE
 ISN 0064              KO=KKK+1
 ISN 0065              IF(KKK.EQ.NP) GO TO 50
 ISN 0067              CALL PLOT(PX(KO),PY(KO),3)
 ISN 0068           50 CONTINUE
 ISN 0069              CALL PLOT(30.0,0.0,-3)
 ISN 0070              CALL LINEWT(-1)
 ISN 0071              CALL SYMBOL(8.0,.50,0.50,3HGAP,0.0,3)
 ISN 0072              CALL PLOT(XOC(1),YOC(1),3)
 ISN 0073              CALL LINEWT(-2)
 ISN 0074              DO 3 I=2,5
 ISN 0075              CALL PLOT(XOC(I),YOC(I),2)
 ISN 0076            3 CONTINUE
 ISN 0077              CALL LINEWT(1)
 ISN 0078              DO 60 I=1,NP
 ISN 0079              XP=CORD(I,2)*COS(PI/18.)-CORD(I,1)*SIN(PI/4.)+DELX
 ISN 0080              YP=CORD(I,2)*SIN(PI/18.)+CORD(I,1)*COS(PI/4.)+DELY
 ISN 0081              HX(I)=XP*CON
 ISN 0082              HY(I)=(H(I)/HSET/10.+YP)*CON
 ISN 0083           60 CONTINUE
 ISN 0084              CALL PLOT(HX(1),HY(1),3)
 ISN 0085              KKK=0
 ISN 0086              DO 75 K=1,J
 ISN 0087              NPOINT=NT(K+1)-NT(K)
 ISN 0088              DO 70 KK=1,NPOINT
 ISN 0089              KKK=KKK+1
 ISN 0090              HXL=HX(KKK)
 ISN 0091              HYL=HY(KKK)
 ISN 0092              CALL PLOT(HXL,HYL,2)
 ISN 0093           70 CONTINUE
 ISN 0094              KO=KKK+1
 ISN 0095              IF(KKK.EQ.NP) GO TO 75
 ISN 0097              CALL PLOT(HX(KO),HY(KO),3)
 ISN 0098           75 CONTINUE
 ISN 0099              CALL LINEWT(0)
 ISN 0100              CALL PLOTND
                    C
                    C
 ISN 0101              RETURN
 ISN 0102              END

PTIONS IN EFFECT*NAME(MAIN) OPTIMIZE(2) LINECOUNT(60) SIZE(MAX) AUTODBL(NONE)

PTIONS IN EFFECT*SOURCE EBCDIC NOLIST NODECK OBJECT NOMAP NOFORMAT GOSTMT NOXREF NOALC NOANSF NOTERM FLAG(I)
```

```
EVEL 2.2.1 (DEC 77)          GRAPH          OS/360  FORTRAN H EXTENDED          DATE 80.088/04.04.1P          PA

TATISTICS*     SOURCE STATEMENTS =     101, PROGRAM SIZE =    26754, SUBPROGRAM NAME = GRAPH

TATISTICS*  NO  DIAGNOSTICS GENERATED

**** END OF COMPILATION *****                                  268K BYTES OF CORE NOT USED

TATISTICS*  NO  DIAGNOSTICS THIS STEP
```